

**LATITUDINAL VARIATION OF METHANE
MEASURED USING A SHIP-BORNE FTIR SPECTROMETER**

MASTER THESIS SUBMITTED BY
HOSSAIN MOHAMMED SYEDUL HOQUE

UNDER THE SUPERVISION OF
PROFESSOR DR. JUSTUS NOTHOLT
DR. MATHIAS PALM

INSTITUTE OF ENVIRONMENTAL PHYSICS (IUP)
UNIVERSITY OF BREMEN

PREFACE

Methane is one of the most important trace gases in the atmosphere. It is regarded as the second most important green house gas. According to IPCC 2007, the global concentration has increased twice since the pre-industrial period. It has a Global Warming potential (GWP) of 72. This means, although less abundant than carbon dioxide methane is 72 times more efficient in trapping outgoing radiation. Despite its importance, the global budget of methane is not yet well understood. Although the sources and sinks of methane are well known, but the flux or strength of the sources and sink are not yet well quantified, as the fluxes vary in space and time. Therefore, methane studies are still challenging in the field of environmental research.

In this study, the measurements taken during a ship cruise in the year 2005 is analyzed and the latitudinal dependence of methane is studied. The latitudinal dependence of trace gases is an important parameter to understand the chemical and dynamical process of the trace gas in the different levels of the atmosphere. It also helps to quantify its transport and impact on the climate.

For the retrieval of the target gas, the retrieval algorithm SFIT4 (v003.94) is used which is based on optimal estimation. The target gas is retrieved in four different ways depending on different spectroscopic line lists and water vapor a priori information. Two spectroscopic line lists are used. One spectroscopic line list is from the HITRAN 2008[Rothman *et.al*, 2008] database which is named as old line list in this work. The second spectroscopic line list is from the Prelim Project [Palm, 2013] which is named as new line list throughout the work. The Prelim Project is an ongoing project which focuses on resolving spectroscopic line parameter more precisely. The project is a joint venture between the Institute of Environmental Physic (IUP), Karschule Institute of Technology (KIT) and German Aerospace Center (DLR). In the new line list the spectral parameters are measured and resolved more precisely than the old line list. So, the quality of retrieval based on the new line list is expected to be good compared to the old line list.

Two different water vapor apriori was also used in the retrieval process. Water vapor apriori from the WCCAM model and NCEP model was used. The difference between the two models is that, NCEP model data are assimilated with measurements. So, the water vapor apriori from the NCEP model is more realistic compared to the WCCAM model.

Based on the spectroscopic line lists and water vapor apriori information, the different retrievals are compared to check the quality of the retrieval and select the best retrieval among them. Then results are compared to previous cruise data and models.

Content

1. Spectroscopy

1.1	Introduction	06
1.2	Review of quantum mechanics	07
1.3	Spectroscopic transition	10
1.4	Line width and resolution	12
1.5	Signal to noise ratio	14
1.6	Microwave Spectroscopy	14
1.7	Infrared Spectroscopy	18

2. Fourier Transform Infrared Spectroscopy

2.1	Introduction	24
2.2	Michelson Interferometer	24
2.3	Mathematical formulation	26
2.4	From infinite to finite resolution	30
2.5	Apodization	32

3. The inverse problem

3.1	What is an inverse problem?	33
3.2	Solution to an inverse problem	33
3.3	Linear problem without measurement error	34
3.4	Linear problem with measurement error	35

4. Aspects about methane

4.1	Introduction	39
4.2	Sources and sinks of methane	39
4.3	Measurement of methane	42
4.3.1	Satellite measurement	42
4.3.2	Ground-based measurement	43

5. Approach of the work

5.1	Introduction	46
5.2	Experimental set-up	47
5.3	CH ₄ retrieval strategy via SFIT4	49
5.4	Analysis Strategy	50
5.5	Total column to column average dry-air mole fraction	51

6. Data analysis

6.1	Preparing measurements	53
6.2	Retrieval	53
6.2.1	Retrieval with old line list	54
6.2.2	Retrieval with new line list	57
6.2.3	Comparison between retrieval with old and new line list	59
6.2.4	Chi-square value	63
6.3	Refine retrieval	65
6.4	Interpretation of results	71

6.5	Model comparison	73
6.6	Conclusion	74

References

1. SPECTROSCOPY*

1.1 Introduction

Spectroscopy is the study of the interaction of electromagnetic radiation with matter. It helps us to obtain detail information regarding molecular structure and chemical properties from atomic and molecular spectra.

An electromagnetic wave of any kind consists of an electric field component ϵ and magnetic field component H .

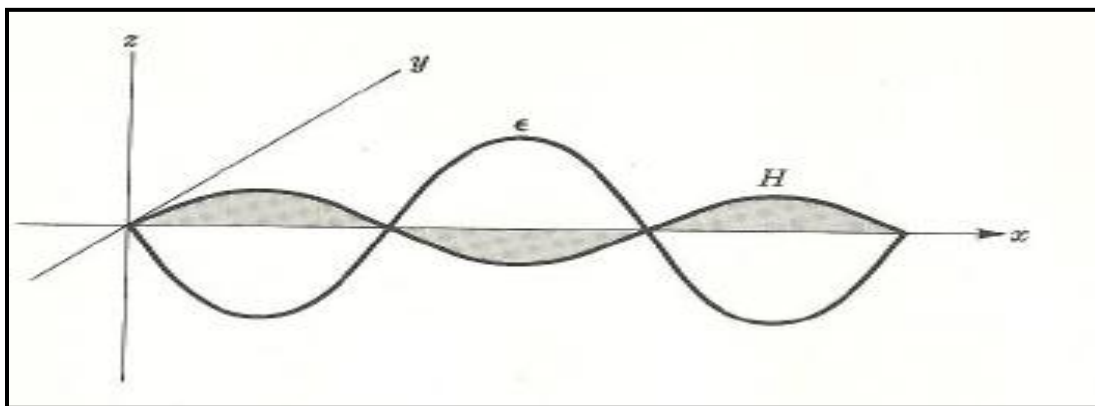


Figure 1.1: The electric and magnetic field component of a plane polarized wave. [Chang]

So the expression for electromagnetic wave travelling in the x direction,

$$\epsilon = \epsilon_0 \sin 2\pi \left(\frac{x}{\lambda} - \nu t \right)$$

$$H = H_0 \sin 2\pi \left(\frac{x}{\lambda} - \nu t \right)$$

Where λ and ν are the wavelength and frequency of the radiation respectively. The velocity of the wave is given by,

$$c = \lambda \nu$$

Thus an electromagnetic wave consists of an electric and a magnetic field oscillating in space. The interaction of electromagnetic wave with matter is either

*This chapter is based on Basic principles of Spectroscopy by Raymond Chang (1971) and Fundamentals of molecular spectroscopy by C.N. Banwell (1996)

with the electric field component and electric field properties or between magnetic component and magnetic properties of the atoms and molecules.

1.2 Review of quantum mechanics

According to Max Planck, absorption and emission of radiation by matter does not take place continuously but in finite quanta of energy. The energy E related to the absorption and emission process is proportional to the frequency ν of the harmonic oscillator.

$$E = h\nu$$

Where h is the Planck's constant.

Again, according to Einstein light consists of quanta of energy $h\nu$, called photons. Photons travel at a velocity of light. When a photon of energy $h\nu$ strikes a surface, electron is emitted with velocity v , and the kinetic energy of the electron is given by,

$$\frac{1}{2}m_e v^2 = h\nu - W$$

Where m_e the mass of the electron and W is the characteristic of the metal.

Later, Bohr postulated that in atoms electrons occupy states or level of different energies. The transition of electron from higher energy level (E_h) to a lower energy state (E_l) causes emission of light.

$$E_h - E_l = \Delta E = h\nu \quad (1.1)$$

The energy associated with such electronic transition is one photon energy i.e. $h\nu$. Conversely, the transition of electron from lower to higher energy level can take place by absorbing a photon.

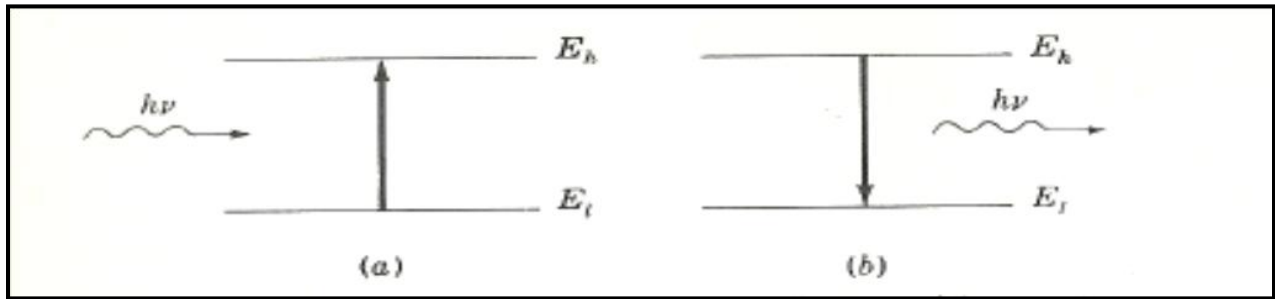


Figure 1.2: Interaction of electromagnetic radiation with matter (a) Absorption. (b) Emission [Chang]

According to de Broglie, the particle property of matter is related to its wave property by the following equation

$$\mathbf{p} = m\mathbf{v} = \frac{h}{\lambda}$$

Where p is the momentum (particle nature), λ is the wavelength (wave nature) and h is the Planck's constant.

Again, Heisenberg stated that, precise determination of conjugate variables of a physical system is impossible. Conjugate variables in classical mechanics are energy and time, position and momentum etc. The uncertainty in simultaneous determination of any two conjugate variable X and Y is

$$\Delta X \Delta Y \sim \hbar \tag{1.2}$$

Where, $\hbar = \frac{h}{2\pi}$

$$\Delta E \Delta t \sim \hbar$$

$$\Delta p \Delta q \sim \hbar$$

Where p is the momentum and q is the position.

A particle with mass m moving with a velocity v along the x axis in a potential field $V(x)$, can be written as

$$\mathbf{T} = \frac{1}{2} \mathbf{m} \left(\frac{d\mathbf{x}}{dt} \right)^2$$

$$\mathbf{E} = \frac{1}{2} \mathbf{m} \left(\frac{d\mathbf{x}}{dt} \right)^2 + \mathbf{V}(\mathbf{x}) = \frac{\mathbf{p}^2}{2\mathbf{m}} + \mathbf{V}(\mathbf{x}) \quad (1.3)$$

Equation (1.3) can be converted to Schrödinger's wave equation by replacing momentum \mathbf{p} with the following operator,

$$\begin{aligned} \mathbf{p} &\rightarrow \frac{\hbar}{i} \frac{d}{d\mathbf{x}} \\ \mathbf{p}^2 &\rightarrow \left(\frac{\hbar}{i} \frac{d}{d\mathbf{x}} \right)^2 = -\hbar^2 \frac{d^2}{d\mathbf{x}^2} \end{aligned} \quad (1.4)$$

Therefore, equation (1.3) becomes,

$$-\hbar^2 \frac{d^2}{d\mathbf{x}^2} + \mathbf{V}(\mathbf{x}) = \mathbf{E} \quad (1.5)$$

Equation (1.5) is an operator equation. To make it complete we write,

$$-\hbar^2 \frac{d^2\psi}{d\mathbf{x}^2} + \mathbf{V}\psi = \mathbf{E}\psi \quad (1.6)$$

Equation (1.6) is called the time-independent Schrödinger equation in one dimension, where ψ is the wave function which describes the wave property of a particle with mass m . In three dimension,

$$\begin{aligned} \nabla^2\psi + \frac{2m}{\hbar^2} (\mathbf{E} - \mathbf{V})\psi &= \mathbf{0} \\ \left(-\frac{\hbar^2}{2m} \nabla^2 + \mathbf{V} \right) \psi &= \mathbf{E}\psi \end{aligned} \quad (1.7)$$

Where, ∇^2 is the laplacian operator which is given by ,

$$\nabla^2 = \frac{\partial^2}{\partial x^2} + \frac{\partial^2}{\partial y^2} + \frac{\partial^2}{\partial z^2}$$

1.3 Spectroscopic Transition

The change of energy levels of electrons in atoms results in to absorption and emission of energy. If absorption and emission take place in the presence of an external field they are called induced absorption and emission. Otherwise, they are called spontaneous absorption and emission.

According to the Boltzmann distribution law, the ratio of the population in states n and m,

$$\frac{N_n}{N_m} = e^{-\left(\frac{E_n - E_m}{kT}\right)} \quad (1.8)$$

Where k is the Boltzmann constant. Let us define the following parameters:

The transition probability per unit time for induced absorption, B_{mn}

The transition probability per unit time for induced emission, B_{nm}

The transition probability per unit time for spontaneous emission, A_{nm}

The density of radiation of frequency ν , $\rho(\nu)$

The number of induced emissions per second = $N_n B_{nm} \rho(\nu)$

The number of induced absorption per second = $N_m B_{mn} \rho(\nu)$

The number of spontaneous emissions per second = $N_n A_{nm}$

At steady state, the rates of emission and absorption are equal,

$$N_m B_{mn} \rho(\nu) = N_n B_{nm} \rho(\nu) + N_n A_{nm}$$

$$\begin{aligned} \rho(\nu) &= \frac{N_n A_{nm}}{B_{nm}(N_m - N_n)} \\ &= \frac{A_{nm}}{B_{nm}} \frac{1}{e^{-\frac{E_h - E_l}{kT}} - 1} \end{aligned} \quad (1.9)$$

According to Planck's radiation law,

$$\rho(\nu) = \frac{8\pi h \nu^3}{c^3} \frac{1}{e^{\frac{h\nu}{kT}} - 1} \quad (1.10)$$

From equation (1.9) and (1.10)

$$\frac{A_{nm}}{B_{nm}} \frac{1}{e^{-\frac{E_h - E_l}{kT}} - 1} = \frac{8\pi h \nu^3}{c^3} \frac{1}{e^{\frac{h\nu}{kT}} - 1}$$

Since $\nu = \nu_{nm}$

$$\frac{A_{nm}}{B_{nm}} = \frac{8\pi h \nu_{nm}^3}{c^3} \quad (1.11)$$

Therefore, the intensity of the absorption line is proportional to the population in the lower state. Besides, the competing effect between induced and spontaneous emission might diminish the intensity of the absorption line. The net absorption intensity is given by,

$$N_m B_{mn} \rho(\nu) - N_n B_{nm} \rho(\nu) = B_{nm} \rho(\nu) (N_m - N_n)$$

Therefore the intensity of a given absorption depends on the difference in the population states m and n if $\rho(\nu)$ is kept constant.

1.4 Line width and resolution

According to classical mechanics, the energy levels of electron in atoms are exactly defined. So electron transitions will give rise to sharp transition lines with no width. But, according to Heisenberg's uncertainty principle, simultaneously energy and time cannot be determined precisely.

$$\Delta E \Delta t \sim \hbar$$

Therefore, transitions will have uncertainty in the energy, which is called the lifetime broadening of spectral lines.

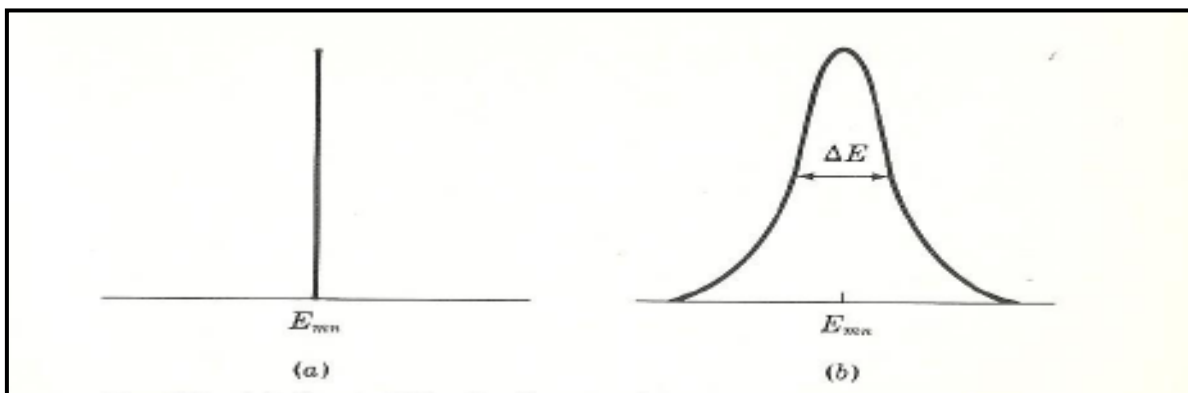


Figure 1.3: (a) Spectral line having no width. (b) Spectral line having width at half height. [Chang]

Spectral lines can also broaden by Doppler effect. This effect comes in to account when a molecule which is measured has a velocity v relative to the measuring instrument. If the molecule is moving towards the instrument with velocity v and the observed frequency of radiation by the molecule is ν' is given by,

$$\nu' = \nu \left(1 + \frac{v}{c}\right)$$

Similarly, if the molecule is moving away from the instrument with velocity v , then ν' is given by,

$$\nu' = \nu \left(1 - \frac{v}{c}\right)$$

Therefore, depending on the direction of the molecule, the observed frequency shifts either toward the higher frequency or lower frequency.

Line broadening also takes place due to collision among atoms, molecules and ions. If the collision time between two species X and Y is longer than the mean collision time, then the energy of absorbing or emitting of X will be influenced by the electric and magnetic field of Y. As a result, the spectral lines of X will be disturbed by this influence. In addition to different mechanism of line broadening, spectral lines can be broadened by the instrument itself also. This is called the resolving power of the instrument i.e. the ability of the instrument to distinguish overlapped lines. It is expressed as the ratio of the observed frequency to the smallest difference between two frequencies that can be measured.

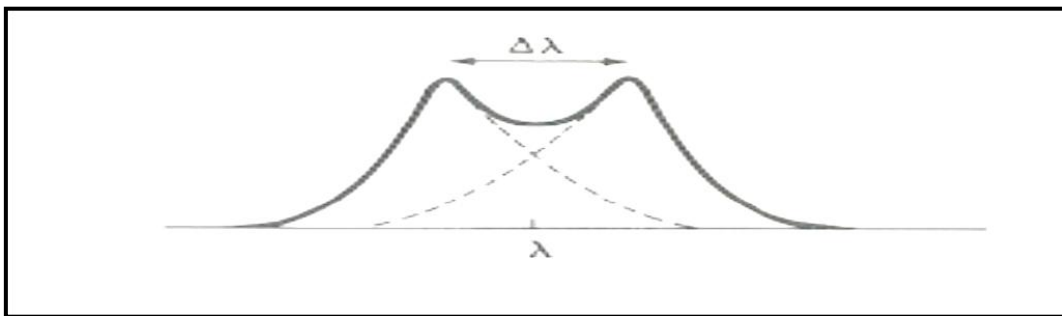


Figure 1.4: Resolving power of a spectrometer. [Chang]

1.5 Signal to noise ratio

Due to the manner in which signals are detected by a spectrometer, recorded spectra always contain random fluctuations of electronic signals. These fluctuations are called noise. The sensitivity depends on the signal to noise ratio i.e. how easily we can distinguish signal from noise. Signals over a certain range are recorded repeatedly and added up. Due to the randomness of the noise, it removes much of the noise level and finally strong signals are obtained.

1.6 Microwave Spectroscopy

Spectroscopy in the microwave region deals with the pure rotational motion of molecules. The condition to observe resonance in the microwave region is that a molecule must possess a permanent dipole moment. The rotating dipole generates an electric field which interacts with the electric field of the microwave radiation. Along with other form of molecular energies, rotational energy is also quantized. That means, a molecule cannot have an arbitrary amount of rotational energy but the energy is limited to certain values depending on the shape and size of the molecule. The permitted energy levels which are called rotational energy levels can be calculated for any molecules solving the Schrödinger equation for the system represented by the molecule. Here, we will consider the simplest of all linear molecules.

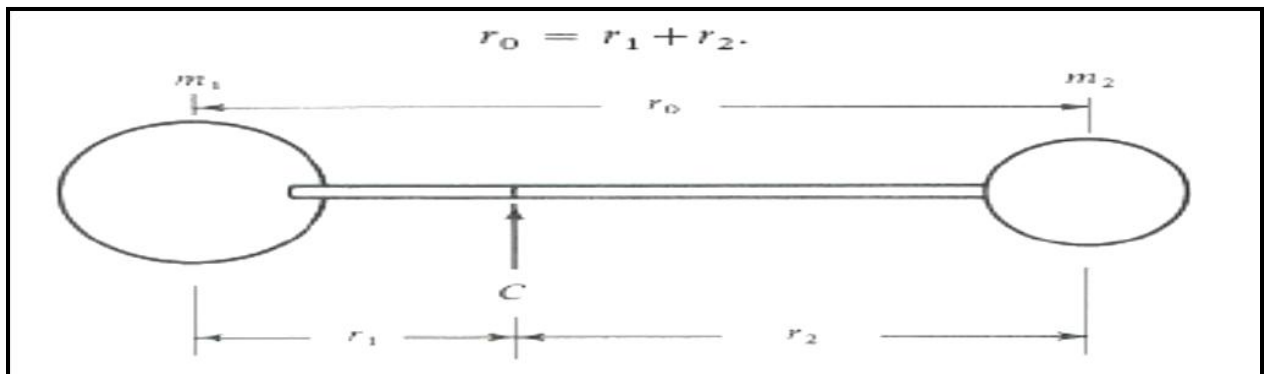


Figure 1.5: A rigid diatomic molecule with two masses m_1 and m_2 joined by a rigid bar of length r_0 .
[Banwel]

Masses m_1 and m_2 are joined by a rigid bar whose length is, $r_0 = r_1 + r_2$

The molecule rotates end-over-end about a point C, the centre of gravity: which is defined by the moment, or balancing, equation:

$$\mathbf{m}_1 \mathbf{r}_1 = \mathbf{m}_2 \mathbf{r}_2 \quad (1.12)$$

The moment of inertia about C is defined by:

$$\begin{aligned} I &= \mathbf{m}_1 \mathbf{r}_1^2 + \mathbf{m}_2 \mathbf{r}_2^2 \\ &= \mathbf{m}_1 \mathbf{r}_1 \mathbf{r}_2 + \mathbf{m}_2 \mathbf{r}_1 \mathbf{r}_2 \\ &= \mathbf{r}_1 \mathbf{r}_2 (\mathbf{m}_2 + \mathbf{m}_1) \end{aligned} \quad (1.13)$$

Again, $\mathbf{m}_1 \mathbf{r}_1 = \mathbf{m}_2 \mathbf{r}_2 = \mathbf{m}_2 (\mathbf{r}_0 - \mathbf{r}_1)$

Therefore,

$$\mathbf{r}_1 = \frac{\mathbf{m}_2 \mathbf{r}_0}{\mathbf{m}_1 + \mathbf{m}_2} \quad \text{And} \quad \mathbf{r}_2 = \frac{\mathbf{m}_1 \mathbf{r}_0}{\mathbf{m}_1 + \mathbf{m}_2} \quad (1.14)$$

Replacing equation (1.14) into (1.13)

$$I = \frac{\mathbf{m}_1 \mathbf{m}_2}{\mathbf{m}_1 + \mathbf{m}_2} \mathbf{r}_0^2 = \mu \mathbf{r}_0^2 \quad (1.15)$$

Where, μ is the reduced mass.

If the rotation is unrestricted, the potential energy $V(\Phi)$ becomes a constant and can be arbitrarily chosen as $V(\Phi) = 0$. The time-independent Schrödinger equation for the rigid diatomic molecules is given by,

$$\nabla^2 \psi + \frac{2IE}{\hbar^2} \psi = 0 \quad (1.16)$$

The solution of equation (1.16) gives,

$$E_J = \frac{h^2}{2I} J(J + 1) \quad (1.17)$$

Where, J is called the rotational quantum number. Equation (1.17) gives the energies in ergs. To find the difference between energy levels or more particularly in corresponding frequency or wave number equation (1.17) is abbreviated to:

$$\varepsilon_j = BJ(J + 1) \quad (1.18)$$

Where, $B = \frac{h}{8\pi^2Ic}$ is the rotational constant .

From equation (1.18) the allowed energy levels can be calculated as shown in figure 1.6

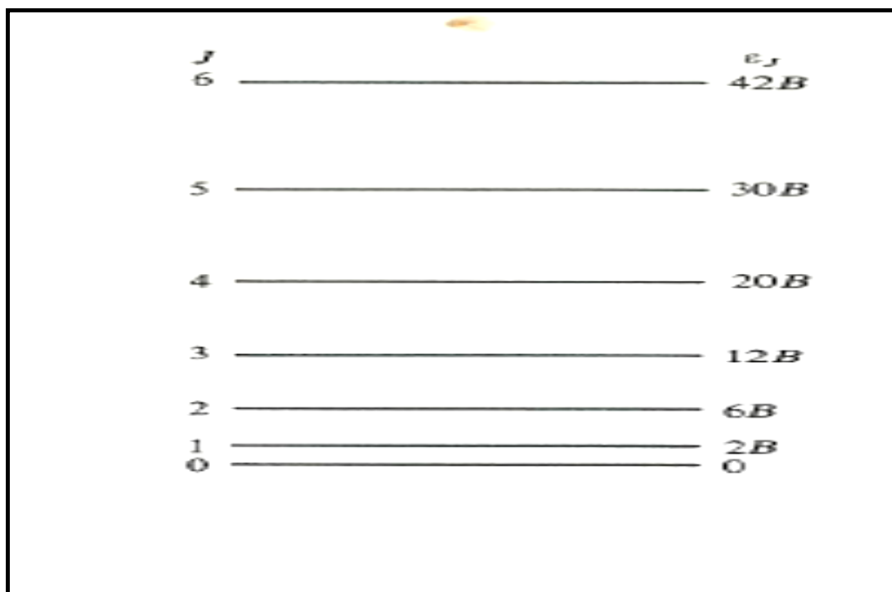


Figure 1.6: The allowed rotational levels for a diatomic molecule. [Banwel]

For $J=0$, $\varepsilon_j = 0$. This means, the molecule is not rotating at all. For $J=1$, $\varepsilon_j = 2B$ and the rotating molecules has the lowest angular momentum. For each value of J the energy levels can be calculated. It seems that, molecules will infinite number of rotational energy levels. But, in reality at a certain point the centrifugal force of

the diatomic atomic molecule will be greater than the strength of the bond. As a consequence the molecule will be disrupted.

To raise the molecule from state J to $J+1$, we have,

$$\begin{aligned} \nu_{J \rightarrow J+1} &= B(J+1)(J+2) - BJ(J+1) \\ &= 2B(J+1) \text{ cm}^{-1} \end{aligned}$$

That means, step-wise raising of the rotational energy results in an absorption spectrum which consists lines at $2B, 4B, 6B \dots$ etc .

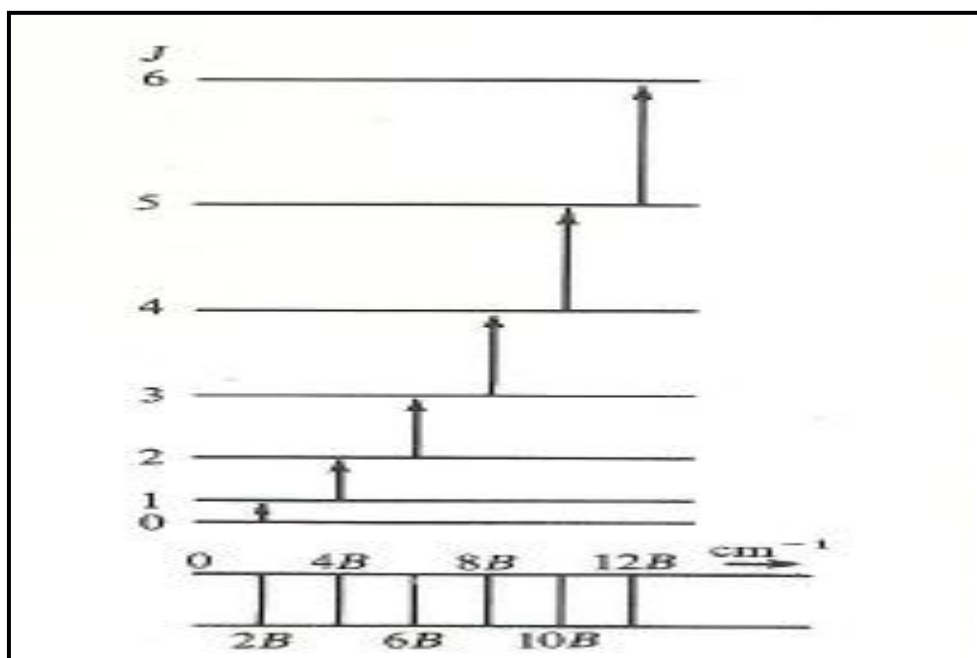


Figure 1.7: The allowed transitions between the energy levels of a rigid diatomic molecule and the Spectrum that arises from the transitions. [Banwel]

To derive this pattern we have made the assumption that a transition can occur from a particular level only to its intermediate neighbor, either above or below. Sophisticated application of Schrödinger wave equation shows that, for a diatomic molecule only the transitions in which J changes by one unit should be

considered. The rest are spectroscopically forbidden. So, the selection rule for a rigid diatomic rotator is:

$$\Delta J = \pm 1$$

1.7 Infrared Spectroscopy

The atoms in a molecule do not remain in fixed relative positions but vibrate about some mean positions. We only consider the case of a diatomic molecule and the spectrum which arises if only motion is vibration.

We assume that, a diatomic molecule behaves like a simple harmonic oscillator. A harmonic oscillator consists of a particle of mass m which is acted upon by a force proportional to its displacement x from an equilibrium position. According to Hooke's law, the force F acting on the particle,

$$\begin{aligned} \mathbf{F} &\propto -x \\ F &= kx \end{aligned}$$

Where, k is the restoring force constant. The potential energy V is given by,

$$V = - \int F dx = \frac{1}{2} kx^2$$

From Newton's second law of motion,

$$\mathbf{F} = m \frac{d^2x}{dt^2} = kx \quad (1.19)$$

The solution of equation (1.19)

$$x = x_0 \sin \sqrt{\frac{k}{m}} t$$

The time-independent Schrödinger equation for the harmonic oscillator,

$$\frac{d^2\psi}{dx^2} + \frac{2m}{\hbar^2} \left(E - \frac{1}{2} kx^2 \right) \psi = 0 \quad (1.20)$$

The solution of equation (1.20)

$$E = \left(v + \frac{1}{2} \right) h \omega_{\text{osc}} \quad (1.21)$$

$$\omega_{\text{osc}} = \frac{1}{2\pi c} \sqrt{\frac{k}{\mu}}$$

Where v is called the vibrational quantum number, ω_{osc} is the oscillation frequency and μ is the reduced mass. Converting to spectroscopic units, we have:

$$\epsilon_v = \left(v + \frac{1}{2} \right) \omega_{\text{osc}} \text{ cm}^{-1} \quad (1.22)$$

Equation (1.22) shows the allowed energy levels for a simple harmonic vibrator.

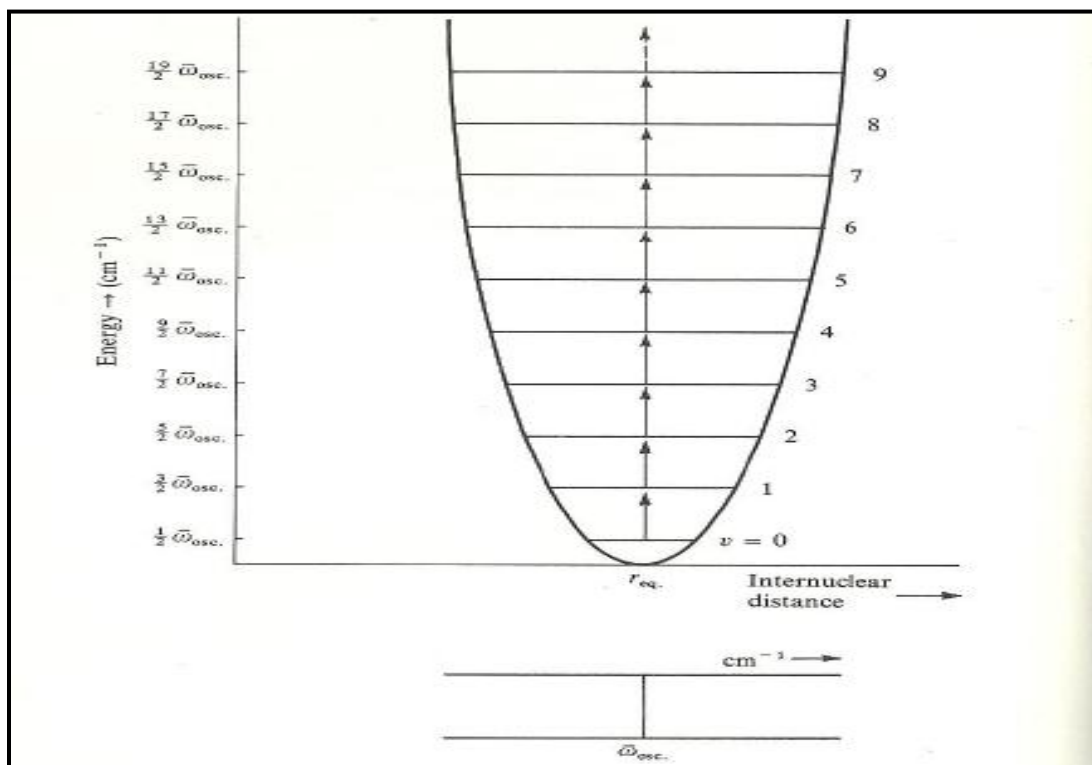


Figure 1.8: The allowed vibrational energy level for a diatomic molecule undergoing harmonic oscillation. [Banwel]

The lowest vibrational energy is obtained by putting $v=0$ in equation (1.22).

$$\epsilon_0 = \frac{1}{2} \omega_{\text{osc}} \text{ cm}^{-1} \quad (1.23)$$

This means that, the diatomic molecule or any other molecule can never have zero vibrational energy. The quantity in equation (1.23) is called zero point energy.

The selection rule for the harmonic oscillator going under vibrational changes:

$$\Delta v = \pm 1$$

Applying the selection rules,

$$\begin{aligned} \epsilon_{v+1 \rightarrow v} &= \left(v + 1 + \frac{1}{2} \right) \omega_{\text{osc}} - \left(v + \frac{1}{2} \right) \omega_{\text{osc}} \\ &= \omega_{\text{osc}} \text{ cm}^{-1} \end{aligned}$$

And for emission,

$$\epsilon_{v \rightarrow v+1} = \omega_{\text{osc}} \text{ cm}^{-1}$$

Real molecules don't obey the law of simple harmonic motion exactly. If the bond between the molecules is stretched, there comes a point at which the molecule disassociates. For small compression and extension the bond may be taken as perfectly elastic but for larger amplitudes-greater than 10 % of the bond length, a much more complicated behavior must be considered. Figure 1.9 shows the energy diagram of a diatomic molecule for a harmonic (dotted) and anharmonic behavior.

The empirical expression which fits the curve to a good approximation is called the Morse function:

$$E = D_{\text{eq}} [1 - \exp\{a(\mathbf{r}_{\text{eq}} - \mathbf{r})\}]^2 \quad (1.23)$$

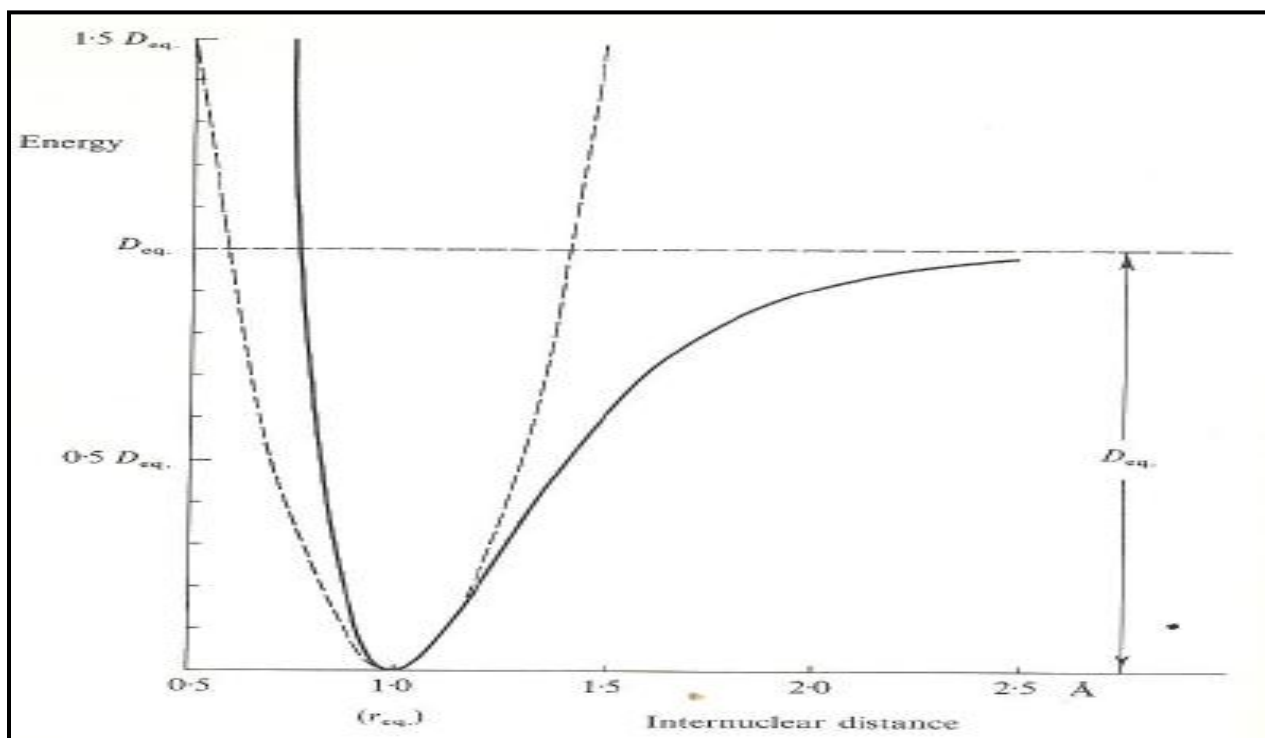


Figure 1.9: Morse curve: energy of a diatomic molecule undergoing anharmonic extensions and compression. [Banwel]

Where a is a constant for a specific molecule and D_{eq} is the dissociation energy. Now the pattern of the allowed vibrational energy level is given by,

$$\epsilon_{v+1 \rightarrow v} = \left(v + 1 + \frac{1}{2} \right) \omega_e - \left(v + \frac{1}{2} \right) \omega_e x_e \quad (1.24)$$

Where ω_e is the oscillation frequency. x_e is the corresponding anharmonicity constant for which bond stretching vibration is always small and positive. So, in the case of the anharmonic oscillator the energy levels will crowd more closely with increasing v .

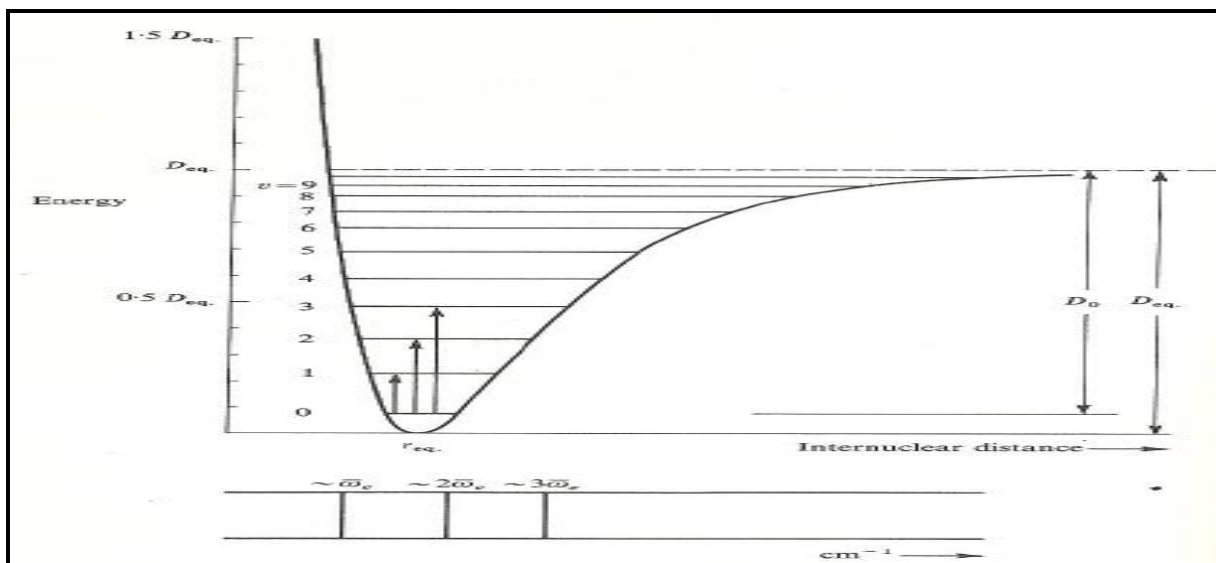


Figure 1.10: The allowed vibrational energy level for a diatomic molecule undergoing anharmonic oscillation . [Banwel]

Re-writing equation (1.24),

$$\varepsilon_v = \omega_e \left\{ 1 - x_e \left(v + \frac{1}{2} \right) \right\} \left(v + \frac{1}{2} \right) \quad (1.25)$$

Comparing equation (1.22) and (1.25)

$$\omega_{osc} = \omega_e \left\{ 1 - x_e \left(v + \frac{1}{2} \right) \right\} \quad (1.26)$$

Therefore the anharmonic oscillator behaves like the harmonic oscillator with an oscillating frequency which decreases with increasing v . Putting $v=-1/2$ in equation (1.26) gives,

$$\omega_{osc} = \omega_e$$

Therefore, ω_e may be defined as the equilibrium oscillation frequency of an anharmonic system. For any real state specified by positive v can be determined by equation (1.26). For example, in the ground state i.e. for $v=0$,

$$\omega_{\text{osc}} = \omega_e \left(1 - \frac{1}{2} x_e \right) \text{ cm}^{-1}$$

$$\varepsilon_0 = \frac{1}{2} \omega_e \left(1 - \frac{1}{2} x_e \right) \text{ cm}^{-1}$$

The selection rule for the anharmonic oscillator going under vibrational changes:

$$\Delta v = \pm 1, \pm 2, \pm 3, \dots$$

2. Fourier Transform Infrared Spectroscopy

2.1 Introduction

FTIR is the short form of Fourier Transform Infra Red, a well known method of infrared spectroscopy. Infrared spectroscopic method produces spectra which represent the molecular absorption and transmission of the sample under experiment. Infrared spectra display the absorption peaks which correspond to the frequencies of vibration of the bonds between atoms the compound is made of. As each material has a unique atomic structure, the infrared spectrum is always a molecular finger print of the compound or sample of interest. As a result, infrared techniques are widely used for identification of materials from spectroscopic analysis. Apart from the identification of compounds and materials, the amount of the materials can also be determined from the size of the peaks in the spectrum. Therefore, infrared spectroscopic techniques are powerful tools for quantitative analysis.

2.2 Michelson Interferometer

Fourier Transform Infrared (FTIR) spectroscopy is a special infrared spectroscopic method which overcomes the limitation of conventional dispersive spectroscopic method. Dispersive instruments scan the frequencies individually, where as FTIR spectrometers scan all the frequencies simultaneously. The most important component of a FTIR spectrometer is the Michelson Interferometer.

*The present chapter is based on the book Fourier Transform Spectrometry by Sumner P. Davis et.al. (2001)

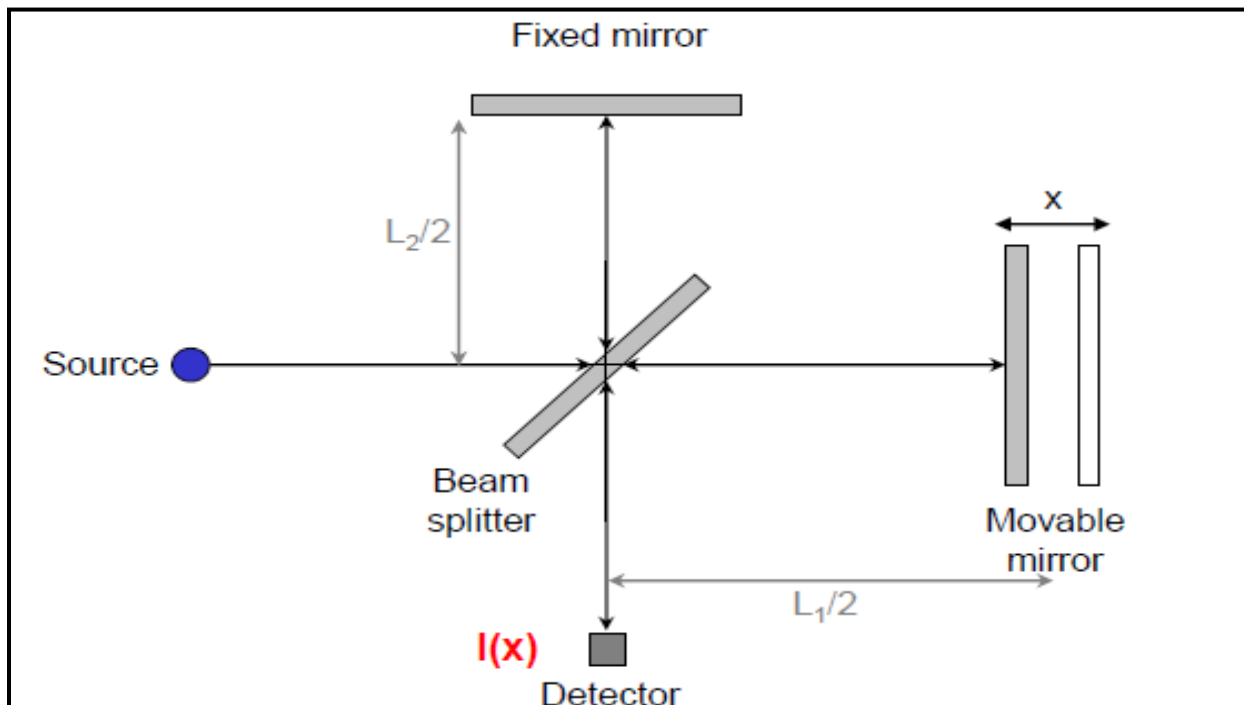


Figure: 2.1 set up of a Michelson Interferometer [Davis et.al.]

Figure 3 shows a schematic view of a Michelson Interferometer. The interferometer consists of a beam splitter, a fixed mirror, a moving mirror, a source of radiation and a detector unit. The source radiates infrared radiation which is collected and collimated and strikes the beam splitter. The beam splitter transmits half of this radiation and reflects the other half. Both the transmitted and reflected radiation encounters mirrors and is reflected back to the beam splitter. Due to the moving mirror, the reflected beams from the mirrors interfere constructively and destructively at the beam splitter. Again half of this radiation is transmitted to the source and the other half is reflected to the detector. The signal measured by the detector is a function of the optical path length difference(OPD). This is called the interferogram.

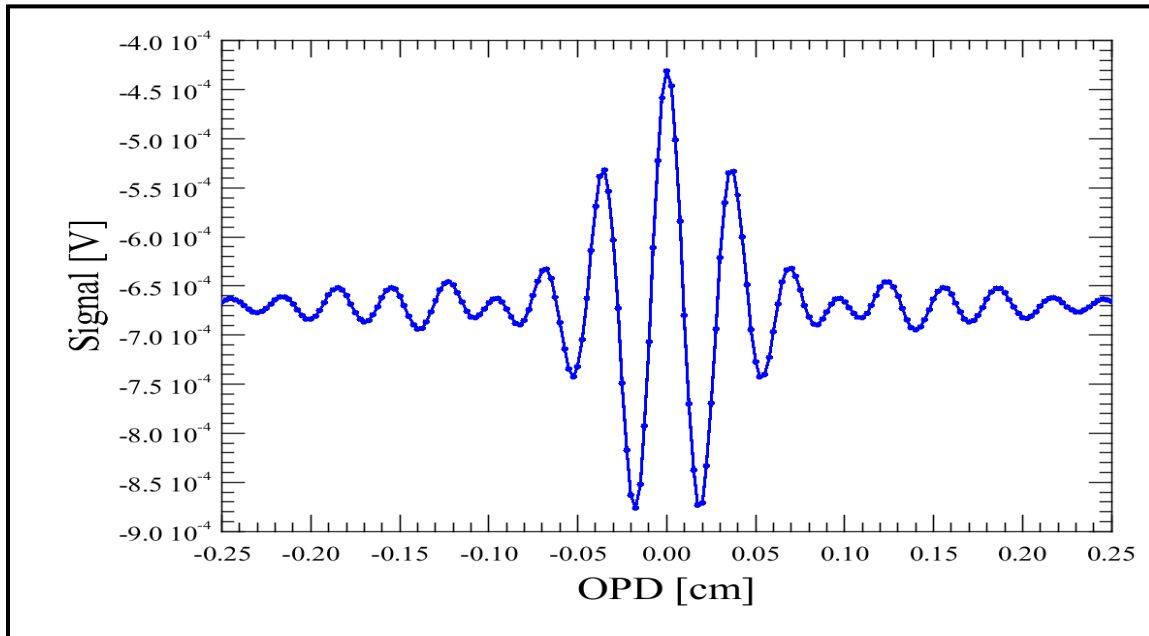


Figure 2.2 : A typical Interferogram

[http://herschel.esac.esa.int/hcss-doc-8.0/load/spire_drg/images/FIGsdumr-SpecifgmSmall.png;
Downloaded on 27/01/2013]

2.3 Mathematical Formulation

The interference of light can be formulated mathematically. The electromagnetic wave expression,

$$E = E_0 \cos(\omega t + \phi)$$

Where, ω is the angular frequency

Φ is the phase

Now, for the interference of two waves with equal amplitude and frequency,

$$E = E_1 + E_2 = E_0 [\cos(\omega t + \phi_1) + \cos(\omega t + \phi_2)]$$

For simpler mathematical calculation, the complex description of light wave is a good choice.

$$\mathbf{E} = \mathbf{E}_0 \mathbf{e}^{i(\omega t + \phi)}$$

For a monochromatic light wave with an electric field vector,

$$\mathbf{E} = \mathbf{E}_0 \mathbf{e}^{i(\omega t + 2\pi \nu x)}$$

Where, $\nu = 1/\lambda = \text{wave number in cm}^{-1}$

Energy in the direction of the detector,

$$\mathbf{E}_D(\delta) = \mathbf{E}_0 \mathbf{e}^{i\omega t} (\mathbf{r}_m \mathbf{r}_m \mathbf{t}_s \mathbf{e}^{i2\pi \nu x_1} + \mathbf{r}_m \mathbf{r}_m \mathbf{t}_s \mathbf{e}^{i2\pi \nu x_2})$$

Where, r_m is the co-efficient of reflection of the mirrors.

r_s is the co-efficient of reflection of the beam splitter.

t_s is the co-efficient of transmission of the beam splitter.

$\delta = x_2 - x_1 = \text{the difference in path length.}$

The intensity of the light measured by the detector,

$$\mathbf{I}_D(\delta) = \mathbf{E}_D^2$$

$$\mathbf{I}_D(\delta) = \mathbf{A} \mathbf{r}_m \mathbf{r}_s \mathbf{t}_s (1 + \mathbf{e}^{i2\pi \nu (x_2 - x_1)} + \mathbf{e}^{-i2\pi \nu (x_2 - x_1)} + 1)$$

$$\mathbf{I}_D(\delta) = \mathbf{A} \mathbf{r}_m \mathbf{r}_s \mathbf{t}_s (2 + \mathbf{e}^{i2\pi \nu \delta} + \mathbf{e}^{-i2\pi \nu \delta})$$

$$\mathbf{I}_D(\delta) = \mathbf{A} \mathbf{r}_m \mathbf{r}_s \mathbf{t}_s (1 + \cos(2\pi \nu \delta))/2$$

Therefore, the intensity detected at the detector is a function of path length by the cosine function. This indicates, this is a periodic function with clear maxima and minima.

If $B(v)dv$ is the energy in the element dv , then in the direction of the detector we have,

$$dI_D(\delta) = B(v)dv(1 + \cos(2\pi v\delta))$$

$$\begin{aligned} I_D(\delta) &= \int_{-\infty}^{\infty} dI \\ &= \int_{-\infty}^{\infty} B(v)dv + \int_{-\infty}^{\infty} B(v)\cos 2\pi v\delta dv \end{aligned}$$

The first integral gives the total energy of the radiation and the second part tells us about the structure of the spectrum. The second part is our interferogram $I(\delta)$.

$$I(\delta) = \int_{-\infty}^{\infty} B(v)\cos 2\pi v\delta dv \quad (2.1)$$

Now, to obtain the spectral irradiance of the source, Fourier transform of the interferogram is performed. As, we know any periodic function can be expanded into its Fourier series.

$$f(x) = \frac{a_0}{2} + \sum_{k=1}^{\infty} (a_k \cos kx + b_k \sin kx)$$

With the Fourier coefficients,

$$\mathbf{a}_k = \frac{1}{\pi} \int_{-\pi}^{\pi} \mathbf{f}(t) \cos(kt) dt$$

$$\mathbf{b}_k = \frac{1}{\pi} \int_{-\pi}^{\pi} \mathbf{f}(t) \sin(kt) dt$$

The Fourier transform of a function $f(x)$ is defined as,

$$\mathbf{F}(y) = \int_{-\infty}^{\infty} \mathbf{f}(x) \mathbf{e}^{i2\pi xy} dx = \mathbf{FT}\{\mathbf{f}(x)\}$$

This integral exists if $f(x)$ and $F(y)$ meets certain conditions. On the reverse side, $f(x)$ can be reconstructed from $F(y)$ using the inverse Fourier transforms \mathbf{FT}^{-1} .

So, the spectral irradiance $B(u)$:

$$\mathbf{B}(u) = \int_{-\infty}^{\infty} \mathbf{I}(\delta) \mathbf{e}^{i2\pi u \delta} d\delta \quad (2.2)$$

As, $I(\delta)$ is a continuous function, it can be written as the sum of odd and even function.

$$\begin{aligned} \mathbf{I}(\delta) &= \frac{1}{2} [\mathbf{I}(\delta) + \mathbf{I}(-\delta)] + \frac{1}{2} [\mathbf{I}(\delta) - \mathbf{I}(-\delta)] \\ &= \mathbf{E}(\delta) + \mathbf{O}(\delta) \end{aligned} \quad (2.3)$$

Insertion of equation (2.3) into (2.2) yields:

$$\mathbf{B}(v) = \int_{-\infty}^{\infty} \mathbf{E}(\delta) \cos 2\pi v \delta \, d\delta - i \int_{-\infty}^{\infty} \mathbf{O}(\delta) \sin 2\pi v \delta \, d\delta \quad (2.4)$$

If the interferogram is a real and even function, the spectrum is real and positive.

$$\begin{aligned} \mathbf{B}(v) &= \int_{-\infty}^{\infty} \mathbf{I}(\delta) \cos 2\pi v \delta \, d\delta \\ &= 2 \int_0^{\infty} \mathbf{I}(\delta) \cos 2\pi v \delta \, d\delta \end{aligned} \quad (2.5)$$

2.4 From infinite to finite resolution

Equation (2.5) shows that measurements with infinite path differences can be obtained. But actual interferometers cannot achieve infinite path differences. This means, Fourier transform cannot be applied to equation 2.3 due to the non-infinite boundaries of practical interferometers ranging from 0 to Δ , where Δ is a finite number. To apply Fourier transform theory to interferometers, we consider a function $f(\delta)$ which is defined as,

$$\begin{aligned} f(\delta) &= 1 \quad \text{if } 0 \leq \delta \leq \Delta \\ &= 0 \quad \text{if } \delta > \Delta \end{aligned}$$

$f(\delta)$ is a truncating function which is multiplied with $\mathbf{I}(\delta)$. This function is widely known as boxcar function. From equation (2.3), the spectrum can be formulated as,

$$\mathbf{T}(v) = \int_{-\infty}^{\infty} \mathbf{I}(\delta) f(\delta) \cos 2\pi v \delta \, d\delta$$

Where, $\mathbf{T}(v)$ is the total Fourier transform of the finite path difference interferogram. Now, the Fourier transform of a product of two functions is equal to the convolution of the Fourier transform of each product:

$$\mathbf{T}(\mathbf{v}) = \mathbf{B}(\mathbf{v}) * \mathbf{F}(\mathbf{v}) = \int_{-\infty}^{\infty} \mathbf{I}(\delta) \mathbf{f}(\delta) \cos 2\pi \nu \delta \, d\delta \quad (2.6)$$

Where, $F(u)$ is the Fourier transform of the boxcar function $f(\delta)$. The convolution part of equation (2.6) yields:

$$\mathbf{B}(\mathbf{v}) * \mathbf{F}(\mathbf{v}) = \int_{-\infty}^{\infty} \mathbf{B}(\mathbf{v}') \mathbf{F}(\mathbf{v}' - \mathbf{v}) \, d\mathbf{v}'$$

The Fourier transform of $F(u)$:

$$\begin{aligned} \mathbf{F}(\mathbf{v}) &= 2\Delta \frac{\sin(2\pi \nu \Delta)}{2\pi \nu \Delta} \\ &= 2\Delta \text{sinc}(2\pi \nu \Delta) \end{aligned}$$

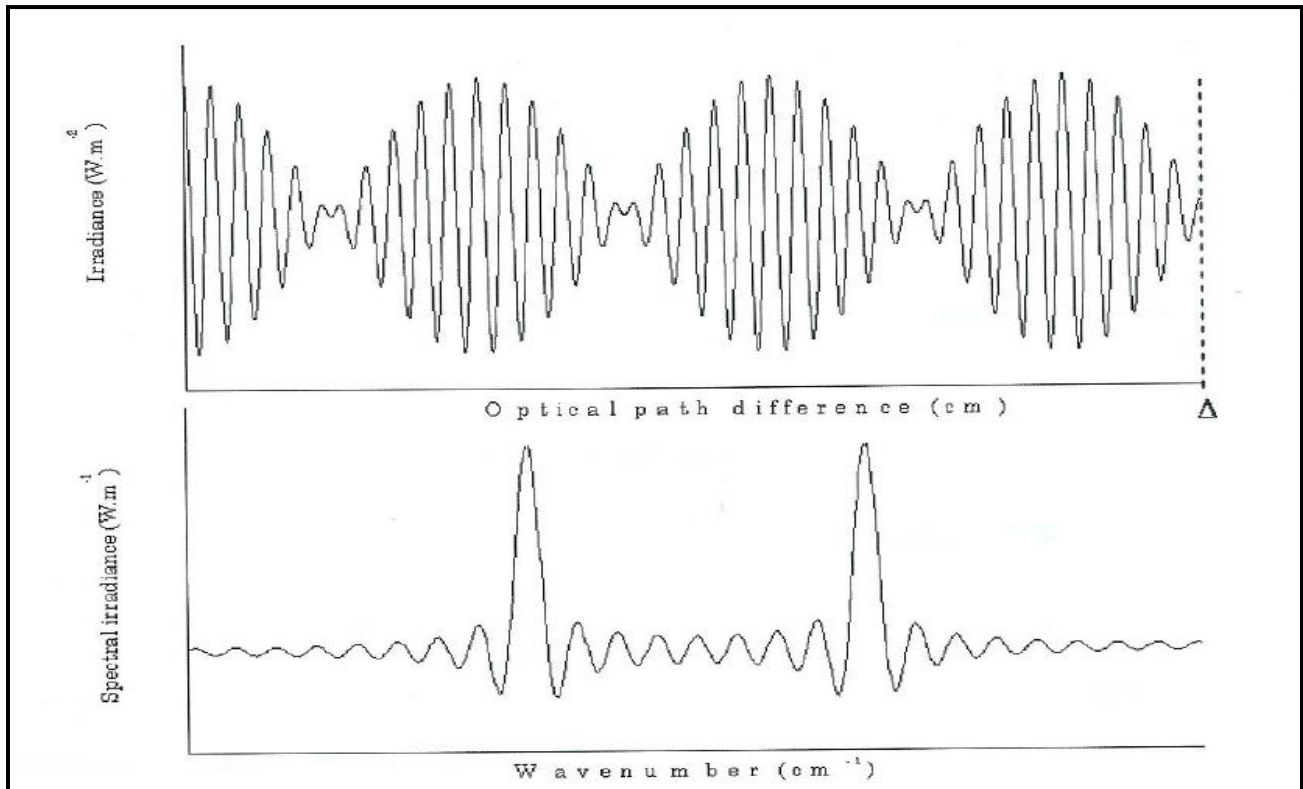


Figure 2.2: An interferogram of finite maximum optical path differences Δ . [Davis et.al.]

The full width at half maximum (FWHM) of the sinc function is called the maximal resolution which can be obtainable theoretically by a Fourier transform spectrometer. It is equal to:

$$R_{theo} = \frac{1.207}{2\Delta} \quad [\text{Davis et.al. 2001}]$$

Where, R_{theo} is the theoretical maximum resolution.

2.5 Apodization

Oscillations of the sinc function can lead to misinterpret of analyzed spectra. In order to avoid misinterpretation, the cut-off of the interferogram at maximum OPD is softened by multiplying it with an apodization function. An apodization function is defined as a weighing function whose value decreases with increasing OPD. As a result, it decreases the effect of truncation of the interferogram at Δ . There is a large variety of Apodization functions and every Apodization function has its own resolution. The apodized maximum spectral resolution R for a triangular function is:

$$R = \frac{1.79}{2\Delta} = \frac{0.9}{\Delta} \quad [\text{Davis et.al. 2001}]$$

3. The inverse problem*

3.1 What is an inverse problem?

In the arena of science, quantities of interest and experiments can be measured in two ways. The direct measurement process and the remote sensing measurement process. Direct measurements are called in situ measurements where the target is directly accessible and the quantity of interest is measured directly from the target using appropriate instruments. Remote sensing measurements are conducted when the target is not directly accessible. In a remote sensing measurement, the quantity actually measured is not the quantity of interest. Rather, it is a complicated function of the parameter that is required. This gives rise to problem of interpretation generally known as inverse problem.

3.2 Solution of an inverse problem

A general inverse problem is regarded as solving set of simultaneous linear or non linear equations with some experimental errors. The information of indirect measurements is assembled in various matrices from where the equations are formed. The measurement vector 'y' contains all the measurements performed. A state vector 'x' contains all the unknown parameters to be resolved. A forward model describes the process or physics behind the measurement process.

For each state vector there will be a corresponding measurement vector which will be determined by the physics of measurement. Therefore, the forward function $F(x)$ can be described as,

$$\mathbf{y} = \mathbf{F}(\mathbf{x})$$

*This chapter is based on Inverse methods for atmospheric sounding by Clive D. Rodgers (2000)

But, in practice all measurement contains errors. Besides, the physics of measurement is determined by the forward model $F(x)$. Therefore, the relation between the measurement vector and the state vector is given by,

$$\mathbf{y} = \mathbf{F}(\mathbf{x}) + \varepsilon$$

Where, vector \mathbf{y} is the measurement with error and $F(x)$ is a vector valued function which determines the physics of measurement.

To examine the information content of the measurement, the forward model is linearised about some reference state \mathbf{x}_0 .

$$\mathbf{y} - \mathbf{F}(\mathbf{x}_0) = \frac{\partial \mathbf{F}(\mathbf{x})}{\partial \mathbf{x}} (\mathbf{x} - \mathbf{x}_0) + \varepsilon = \mathbf{K}(\mathbf{x} - \mathbf{x}_0) + \varepsilon$$

\mathbf{K} is the weighting function matrix with size of $m \times n$. Each element in \mathbf{K} is the partial derivative of a forward model element with respect to a state vector element. If $m < n$, the number of measurements are less than the number of unknowns. This type of system is called under-determined system. On the contrary, for $m > n$, systems are called over-determined system.

3.3 Linear problem without measurement error

If we consider, a linear problem without any measurement errors, the problem reduces to the exact solution of linear simultaneous equations.

$$\mathbf{y} = \mathbf{Kx} \tag{3.1}$$

Then for various conditions, such as over determined, under determined system, no solution, one solution, infinite solutions, etc the equations are solved to determine the unknown parameters. The row space of \mathbf{K} is identified by describing an orthogonal set of vectors that every k_j can be expressed in terms of, which therefore must be an orthogonal set of linear combination of the k_j . This is

done by a process called Singular Value Decomposition (SVD). Matrix K is resolved into 3 different matrices.

$$\mathbf{K} = \mathbf{UAV}^T \quad (3.2)$$

the dimension of U and V are $m \times p$ and $n \times p$ and A is a $p \times p$ diagonal matrix of non-zero singular values, where p is the rank of K . Inserting equation (3.2) in equation (3.1)

$$\mathbf{y} = \mathbf{UAV}^T \mathbf{x} \quad (3.3)$$

Multiplying equation (3.3) by U^T gives

$$U^T \mathbf{y} = \mathbf{AV}^T \mathbf{x}$$

$$\mathbf{y}' = \mathbf{Ax}' \quad (3.4)$$

Where $\mathbf{y}' = U^T \mathbf{y}$ and $\mathbf{x}' = V^T \mathbf{x}$. Equation (3.4) shows that, p transformed measurements \mathbf{y}' in column space, are each proportional to a component of a transformed state \mathbf{x}' in p -dimensional row space.

3.4 Linear problem with measurement error

Measurements in the real world are subjected to errors. So, the retrieval algorithms should allow for errors or noise. Generally, experimental errors are described in terms of probability density function (pdf) and Bayesian approach to probability gives us useful insight to solve inverse problems with errors. If a scalar measurement has a value \bar{y} and error σ , then our knowledge of the true value of measured parameter is described by pdf $P(y)$ with a mean \bar{y} and variance σ^2 .

$$\bar{y} = \int y P(y) dy$$

$$\sigma^2 = \int (y - \bar{y})^2 P(y) dy \quad (3.5)$$

The form of $P(y)$ is almost always considered to be Gaussian distributed or normally distributed.

$$\mathbf{P}(\mathbf{y}) = \mathbf{N}(\mathbf{y} - \bar{\mathbf{y}}, \sigma) = \frac{1}{(2\pi)^{1/2}\sigma} \exp\left\{-\frac{(y-\bar{y})^2}{2\sigma^2}\right\} \quad (3.6)$$

For a measured vector quantity the probability density function can be defined over measurement space, $P(y)$, where $P(y) dy$ is the probability true value of measurement lies in the interval $(y, y+dy)$ in the measurement space. Different elements of the vector may be correlated by,

$$\mathbf{S}_{ij} = \mathbf{E}\{(\mathbf{y}_i - \bar{\mathbf{y}}_i)(\mathbf{y}_j - \bar{\mathbf{y}}_j)\} \quad (3.7)$$

Where, S_{ij} is the covariance of y_i and y_j , and E is the expected value operator. These covariences are assembled into a matrix, called the covariance matrix S_y of the measurement vector y . The diagonal elements of a covariance matrix are the variance of the individual elements of y . So, the Gaussian distribution for a vector is:

$$\mathbf{P}(\mathbf{y}) = \frac{1}{(2\pi)^{n/2} S_y^{1/2}} \exp\left\{-\frac{1}{2}(\mathbf{y} - \bar{\mathbf{y}})^T \mathbf{S}_y^{-1}(\mathbf{y} - \bar{\mathbf{y}})\right\} \quad (3.8)$$

Again, S_y can be decomposed using the Singular Value decomposition method.

$$\begin{aligned} \mathbf{P}(\mathbf{y}) &= \frac{1}{(2\pi)^{n/2} (\mathbf{LAL}^T)^{1/2}} \exp\left\{-\frac{1}{2}(\mathbf{y} - \bar{\mathbf{y}})^T (\mathbf{LAL}^T)^{-1}(\mathbf{y} - \bar{\mathbf{y}})\right\} \\ &= \frac{1}{(2\pi)^{n/2} (\mathbf{A})^{1/2}} \exp\left\{-\frac{1}{2}(\mathbf{z})^T (\mathbf{A})^{-1}\mathbf{z}\right\} \end{aligned}$$

Where, $\mathbf{z} = \mathbf{L}^T(\mathbf{y} - \bar{\mathbf{y}})$

Now, we adopt the Bayesian approach to try to solve the noisy inverse problem. We have a prior knowledge of a quantity and we want to update the understanding with help of new information. Imperfect prior knowledge is quantified as a pdf over the state space and the measurement with error can be quantified as a pdf over the measurement space. Now, Bayes theorem tells us

how the measurement pdf maps into state space and combines with our prior knowledge. Bayes theorem for vector case is given by.

$$\mathbf{P}(\mathbf{x}|\mathbf{y}) = \frac{\mathbf{P}(\mathbf{y}|\mathbf{x})\mathbf{P}(\mathbf{x})}{\mathbf{P}(\mathbf{y})} \quad (3.9)$$

The left hand side of equation (3.9) is the posterior pdf of the state when the measurement is given. This is what we want to update our prior knowledge $\mathbf{P}(\mathbf{x})$ based on the measurement. $\mathbf{P}(\mathbf{y}|\mathbf{x})$ describes the knowledge of \mathbf{y} , if the state is \mathbf{x} . $\mathbf{P}(\mathbf{y}|\mathbf{x})$ can be written explicitly with the forward model $\mathbf{F}(\mathbf{x})$ and the error description.

$$\mathbf{P}(\mathbf{y}|\mathbf{x}) = \exp\{-\mathbf{(\mathbf{y} - \mathbf{F}(\mathbf{x}))}^T \mathbf{S}_\varepsilon^{-1} (\mathbf{y} - \mathbf{F}(\mathbf{x}))\} \quad (3.10)$$

Where, \mathbf{S}_ε is the measurement error covariance matrix. For a linear problem, the forward model is also linear.

$$\mathbf{y} = \mathbf{F}(\mathbf{x}) + \varepsilon = \mathbf{K}\mathbf{x} + \varepsilon \quad (3.11)$$

So equation (3.10) can be expressed as,

$$-2\ln\mathbf{P}(\mathbf{y}|\mathbf{x}) = (\mathbf{y} - \mathbf{K}\mathbf{x})^T \mathbf{S}_\varepsilon^{-1} (\mathbf{y} - \mathbf{K}\mathbf{x}) + \mathbf{c}_1 \quad (3.12)$$

Where, \mathbf{c}_1 is a constant. The prior knowledge of \mathbf{x} can also be described by a Gaussian pdf:

$$-2\ln\mathbf{P}(\mathbf{x}) = (\mathbf{x} - \mathbf{x}_a)^T \mathbf{S}_a^{-1} (\mathbf{x} - \mathbf{x}_a) + \mathbf{c}_2 \quad (3.13)$$

Where, \mathbf{x}_a is the a priori value of \mathbf{x} and \mathbf{S}_a is the covariance matrix of \mathbf{x} .

Now, substituting equation (3.12) and (2.13) in equation (3.9)

$$-2\ln\mathbf{P}(\mathbf{x}|\mathbf{y}) = (\mathbf{y} - \mathbf{K}\mathbf{x})^T \mathbf{S}_\varepsilon^{-1} (\mathbf{y} - \mathbf{K}\mathbf{x}) + (\mathbf{x} - \mathbf{x}_a)^T \mathbf{S}_a^{-1} (\mathbf{x} - \mathbf{x}_a) + \mathbf{c}_3 \quad (3.14)$$

Equation (3.14) is a quadratic form in \mathbf{x} . So, it can be rewritten as,

$$-2\ln P(\mathbf{x}|\mathbf{y}) = (\mathbf{x} - \hat{\mathbf{x}})^T \hat{\mathbf{S}}^{-1} (\mathbf{x} - \hat{\mathbf{x}}) + \mathbf{c}_4 \quad (3.15)$$

That means the posterior pdf is a Gaussian distribution with expected value $\hat{\mathbf{x}}$ and covariance $\hat{\mathbf{S}}$. Now, equation (3.14) and (3.15) can be related by equating the similar terms. Equating the term that are quadratic in \mathbf{x} :

$$\begin{aligned} \mathbf{x}^T \mathbf{K}^T \mathbf{S}_\varepsilon^{-1} \mathbf{K} \mathbf{x} + \mathbf{x}^T \mathbf{S}_a^{-1} \mathbf{x} &= \mathbf{x}^T \hat{\mathbf{S}}^{-1} \mathbf{x} \\ \hat{\mathbf{S}}^{-1} &= \mathbf{K}^T \mathbf{S}_\varepsilon^{-1} \mathbf{K} + \mathbf{S}_a^{-1} \end{aligned} \quad (3.16)$$

Now, equating the terms linear in \mathbf{x}^T :

$$(-\mathbf{K}\mathbf{x})^T \mathbf{S}_\varepsilon^{-1} (\mathbf{y}) + (\mathbf{x})^T \mathbf{S}_a^{-1} (-\mathbf{x}_a) = \mathbf{x}^T \hat{\mathbf{S}}^{-1} (-\hat{\mathbf{x}}) \quad (3.17)$$

Inserting the value of equation (3.16) in (3.17)

$$\begin{aligned} \mathbf{K}^T \mathbf{S}_\varepsilon^{-1} \mathbf{y} + \mathbf{S}_a^{-1} \mathbf{x}_a &= (\mathbf{K}^T \mathbf{S}_\varepsilon^{-1} \mathbf{K} + \mathbf{S}_a^{-1}) \hat{\mathbf{x}} \\ \hat{\mathbf{x}} &= (\mathbf{K}^T \mathbf{S}_\varepsilon^{-1} \mathbf{K} + \mathbf{S}_a^{-1})^{-1} + (\mathbf{K}^T \mathbf{S}_\varepsilon^{-1} \mathbf{y} + \mathbf{S}_a^{-1} \mathbf{x}_a) \\ &= \mathbf{x}_a + (\mathbf{K}^T \mathbf{S}_\varepsilon^{-1} \mathbf{K} + \mathbf{S}_a^{-1})^{-1} \mathbf{K}^T \mathbf{S}_\varepsilon^{-1} (\mathbf{y} - \mathbf{K}\mathbf{x}_a) \end{aligned} \quad (3.18)$$

An alternate form of equation (3.18) is:

$$\hat{\mathbf{x}} = \mathbf{x}_a + \mathbf{S}_a \mathbf{K}^T (\mathbf{K} \mathbf{S}_a \mathbf{K}^T + \mathbf{S}_\varepsilon)^{-1} (\mathbf{y} - \mathbf{K}\mathbf{x}_a) \quad (3.19)$$

So, therefore the Bayesian solution of an inverse problem is the Gaussian pdf $P(\mathbf{x}|\mathbf{y})$ of which $\hat{\mathbf{x}}$ is the expected value and $\hat{\mathbf{S}}$ is the co variancematrix.

4. ASPECTS ABOUT METHANE

4.1 Introduction

Methane is the simplest alkenes chemical compound. It is the main component of natural gas and the most abundant organic compound on earth. In the field of environmental science and research, methane is of prime important for being a green house gas. It is one of the most important green house gases in the atmosphere. Besides, it also among the target species marked by the Kyoto Protocol. [Foster et al., 2007]. Methane in its gas phase is characterized spectroscopically by its highly infrared active eigen modes due to the tetrahedral molecular structure. As a result it has a global warming potential of 72 in the earth's atmosphere over a period of 20 years. [Sussman et al., 2011]. Global warming potential (GWP) is relative measure of the ability of a green gas to trap outgoing radiation. It compares the heat trapping ability of a certain mass of a gas to the same amount of heat trapped by the similar amount of carbon dioxide. GWP of 72 means that, for the existence of similar amount of methane and carbon dioxide in the atmosphere, methane will trap heat 72 times more efficiently than carbon dioxide over the period of twenty years. Therefore, being 200 times less abundant than carbon dioxide, methane is 72 times more efficient in trapping long wave radiation on a 20 year time scale. The change in the methane mixing ratio since the pre-industrial period to 2005 gives a radiative forcing of $+0.48 \pm 0.05 \text{ Wm}^{-2}$ which ranks methane as the second highest radiative forcing of the green house gases after carbon dioxide. [Sepulveda et al., 2012]. Methane has strong infrared (IR) absorption at $7.66\mu\text{m}$, where carbon dioxide and water absorb weakly. Therefore it has a direct effect on the radiative balance of the atmosphere. [Dlugokencky et al. , 1994].

4.2 Sources and Sinks of methane

Methane originates from both biogenic and non biogenic sources. The main sources producing methane are considered to be biogenic formation of methane occurring in natural wetlands, water-flooded rice paddies, landfills,

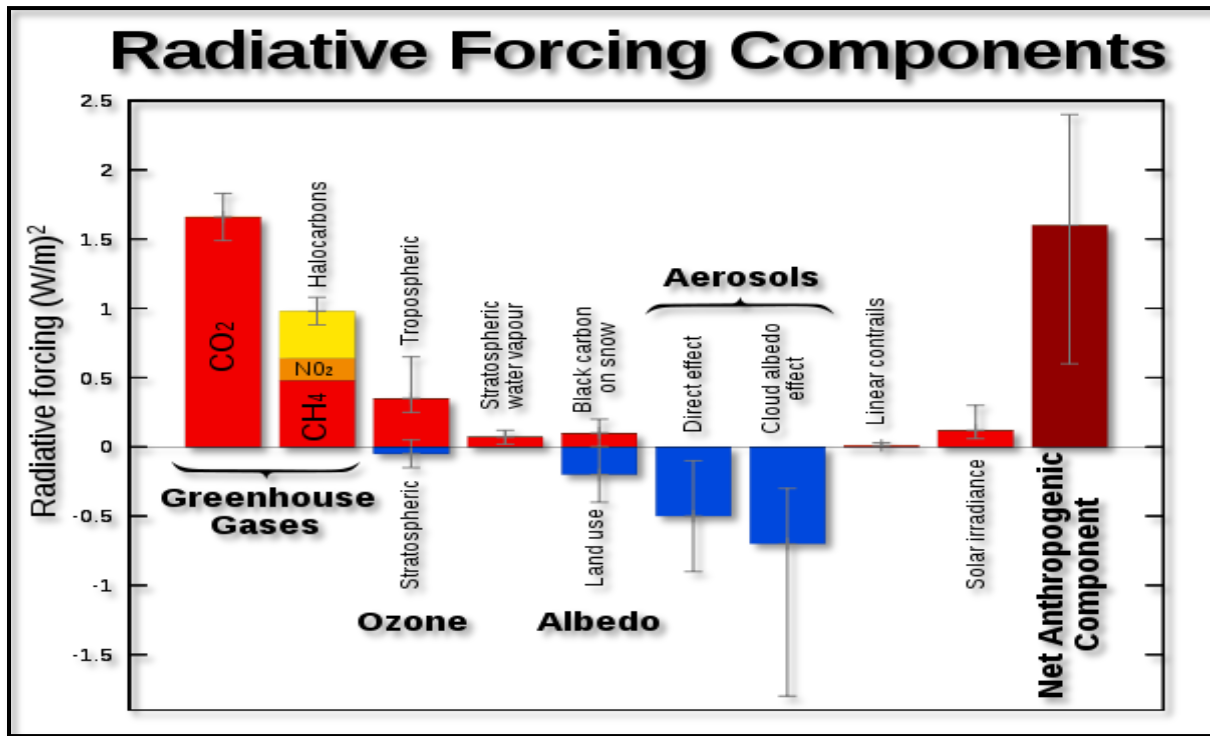
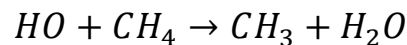


Figure 4.1: Radiative Forcing of atmospheric components. [Foster et.al., 2007]

stomach of ruminant animals, ocean and vegetation. [Sepulveda et al., 2012]. Non biogenic sources include fossil fuel combustion, biomass burning and geological sources. [Foster et al., 2007]. Further sources are released from melting permafrost and shallow hydrates on the continental shelf. [Sepulveda et al., 2012]. Over geological time scales, natural gas deposits are generated by the process of thermogenic formation. Parts of this inventory are released into the atmosphere due to extraction, processing, transportation and distribution of fossil fuel. [Sepulveda et al., 2012]. 70% of the total global emission is accounted by biogenic sources. [Foster et al., 2007].

The main sink of atmospheric methane is the reaction with hydroxyl radical. About 90% of methane is removed by oxidation in the troposphere [Sepulveda et al., 2012]. The process is initiated by reaction with the hydroxyl radical:



This reaction is the second step of the reaction of HO with carbon monoxide as a loss process of OH [*Dlugokencky et al. , 1994*]. The oxidization of methane involves five key intermediate species CH_3 , CH_3O_2 , CH_2O and HCO . The other species include $\text{O}(^1\text{D})$, Cl , NO , NO_2 , HO_2 and O_2 . These species play an important role in determining the oxidization capacity of the atmosphere. Methane oxidization eventually leads to the formation of CO_2 and may also produce O_3 under conditions when the nitric oxide (NO) concentration is greater than 5 to 10 ppt. As these two gases (CO_2 and O_3) are green house gases methane oxidization has an indirect effect on climate. [*Dlugokencky et al. , 1994*]. Besides reaction with hydroxyl radicals, the rest of the sink of methane are uptake by soils, reaction with Cl in the marine boundary layer and transport into the stratosphere, where it is decomposed by reaction with OH , $\text{O}(^1\text{D})$ and Cl . [*E. Sepulveda et al., 2012*]. The reaction of methane with Cl is important, as it isolates reactive chlorine in a temporary reservoir , HCl molecules , which do not destroy ozone. . [*Dlugokencky et al. , 1994*].

The present atmospheric level of methane is still not so clear. The global direct measurement of methane in the atmosphere reveals, that in the last three decades the growth rate of methane has shown substantial downwards trends despite of the 30% increase in the same time span. The slow down decrease of concentration growth of methane started in the late 80's starting from 14ppby^{-1} to almost close to zero in between 1999 and 2005. *Foster et al., 2007*

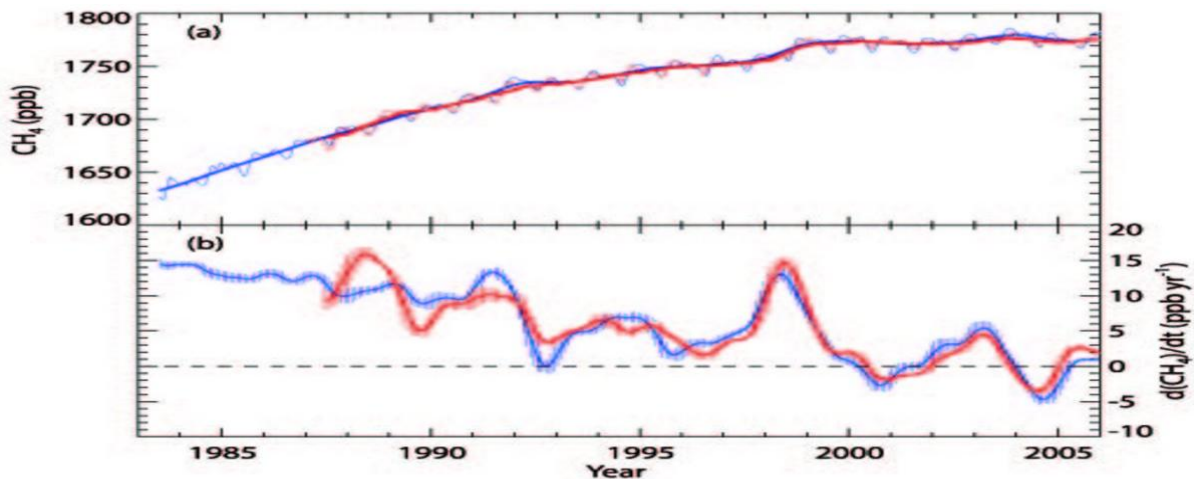


Figure 4.2: Concentration on trends of global atmospheric methane red curve derived from NOAA/GMD Network and the blue Curve from AGAGE network. [*Foster et al., 2007*].

The reasons for decrease in the atmospheric CH₄ growth rate and the implications for future change in its atmospheric burden are not yet well understood. But, it is clear that the changes are related to the imbalance between CH₄ sources and sinks. [Foster et al., 2007]. The reason is not that, sources are not well known. The absolute strengths of many of these sources are not yet well known and difficult to quantify. For example, methane emissions from natural wetlands in Alaska were studied during the Arctic Boundary Layer Experiment (ABLE). It was found that, CH₄ fluxes vary considerably in space and time, as they depend on many natural and anthropogenic factors. [Dlugokencky et al. , 1994]. Figure 4.3 shows the sources and sinks of methane in addition to their atmospheric budget.

4.3 Measurement of Methane

Methane in the atmosphere can be measured from can be observed from instruments from space or from ground base instruments. Here we discuss some methods of measuring atmospheric methane.

4.3.1 Satellite Measurement

The total column of methane (CH₄) can be determined from space borne measurements available from Scanning Imaging Absorption Spectrometer for Atmospheric Cartography (SCIAMACHY) which is on board ENVISAT. [Schneising et.al., 2009]. This instrument makes nadir observation in the near- infrared (NIR wavelength range: 0.8-2.3μm). The target species are the important green house gases such as water vapor, methane, carbon dioxide, carbon monoxide and nitrous oxide. SCIAMACHY is one of the first satellites to measure green house gases on global scale. The advantage of near infrared measurement over thermal infrared measurement is the sensitivity in the boundary layers. Near infrared instruments are more sensitive near the earth surface, where the majority of the emission sources lie compared to the reduced sensitivity of the thermal infrared measurements. The total column is retrieved from the measurements using different algorithms. Retrieval algorithms used for SCIAMACHY data are Weighting Function Modified Differential Optical Absorption Spectroscopy

(WFMDOAS)(version 0.5 for CO and CH₄), Iterative Maximum a Posteriori Differential Optical Absorption Spectroscopy (IMAP-DOAS). [Dils, et al., 2006]

4.3.2 Ground based measurement

Methane is also measured with ground based instruments using FTIR spectrometers. These measurements are made by setting station at different locations around the globe and creating a network. Such a type of network of is the Network for the Detection of Atmospheric Composition Change (NDACC). This network has more than seventy remote sensing stations to observe the physical and chemical state of the stratosphere and the upper troposphere. (<http://www.ndacc.org/>) The infrared working group (IRWG) is a part of NADCC which represents a network of Fourier transform spectrometers. Around twenty high resolution spectrometers measure the absorption spectrum of atmospheric gases regularly. These spectra are used to determine the concentration of atmospheric constituents such as methane, ozone, nitric acid, hydrogen fluoride, carbon monoxide, etc. (<http://www.ndacc.org/>)

To retrieve the concentration from the measured spectra, the measured spectrum is compared with a simulated spectrum. Based on the apriori information of the atmosphere (temperature and pressure profiles) and considering the instrumental influences, a transmission spectrum for the atmosphere is calculated. Then varying various parameters the calculated spectrum is fitted to the measured spectrum. Total column of trace gas concentration can be obtained by scaling the trace gas concentration profiles during the fit. Ground base measurement data are also compared with satellite measurements for validation. The purpose of validation is to check the consistency and the quality of the measurements. [Petersen et al., 2010]. Ground-based high resolution FTIR measurements determine the atmospheric abundances i.e. total column and amounts and vertical profiles of many

	Indicative ¹³ C , ‰ ^b	Hein et al., 1997 ^c	Houwelin g et al., 2000 ^c	Olivie r et al., 2005	Wuebble s and Hayhoe, 2002	Scheehl e et al., 2002	J. Wang et al., 2004 ^c	Mikalof f Fletche r et al., 2004a ^c	Chen and Prinn , 2006 ^c	TAR	AR4
Base year		1983 – 1989		2000		1990	1994	1999	1996 – 2001	1998	2000 – 2004
Natural sources			222		145		200	260	168		
Wetlands	–58	231	163		100		176	231	145		
Termites	–70		20		20		20	29	23		
Ocean	–60		15		4						
Hydrates	–60				5		4				
Geological sources	–40		4		14						
Wild animals	–60		15								
Wildfires	–25		5		2						
Anthropogenic sources		361		320	358	264	307	350	428		
Energy						74	77				
Coal mining	–37	32		34	46			30	48 ^d		
Gas, oil, industry	–44	68		64	60			52	36 ^e		
Landfills & waste	–55	43		66	61	69	49	35			
Ruminants	–60	92		80	81	76	83	91	189 ^f		
Rice agriculture	–63	83		39	60	31	57	54	112		
Biomass burning	–25	43			50	14	41	88	43 ^e		
C3 vegetation	–25			27							
C4 vegetation	–12			9							
Total sources		592			503		507	610	596	598	582
Imbalance		+33								+22	+1
Sinks											
Soils	–18	26			30		34	30		30	30 ^g
Tropospheric OH	–3.9	488			445		428	507		506	511 ^g
Stratospheric loss		45			40		30	40		40	40 ^g
Total sink		559			515		492	577		576	581^g

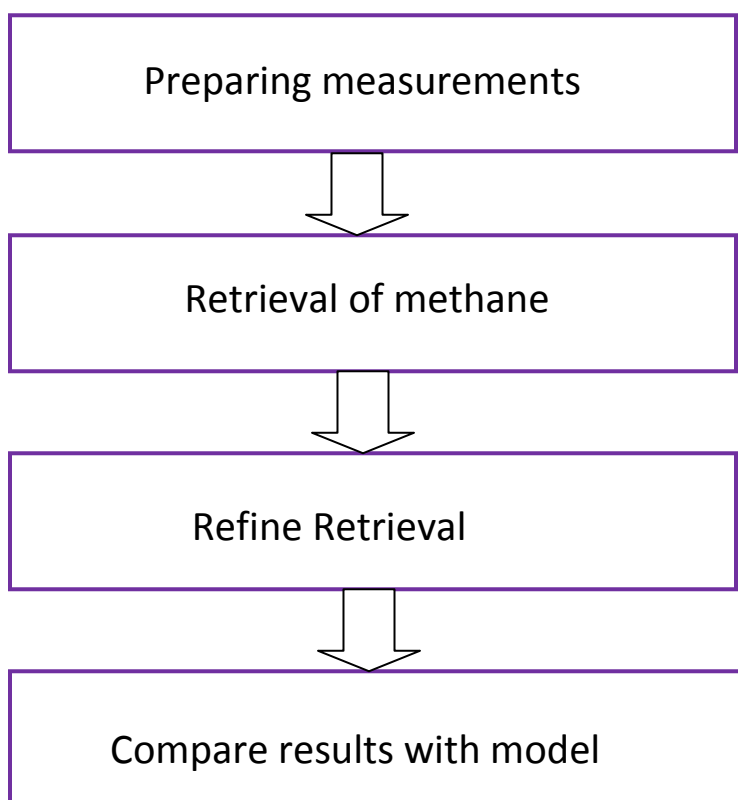
Figure 4.3: Sources, sinks and atmospheric budget of methane. (Foster et.al., 2007)

atmospheric constituents. Total column averaged observations are significantly less affected by small scale processes compared to in-situ surface measurements. In situ surface measurements show very high precision and absolute accuracy(almost 0.1%), but they are strongly affected by small scale turbulences or local source and sinks. However, total column averaged data are affected by stratospheric contribution, which gives rise to significant errors during studies of green house gas cycling between the atmosphere , the biosphere and the ocean. Ground-based FTIR total column data are essential for the validation of satellite measurements of green house gases. [*Sepulveda et al., 2012*]. By means of ground-based FTIR vertical profile data, tropospheric column average mixing ration can be calculated. These ratios are not affected by small scale near surface processes and stratospheric contributions. With high precision and accuracy, tropospheric column averaged mixing ratios are used to investigate green house gas cycling between the atmosphere, the biosphere and the ocean. [*Sepulveda et al., 2012*].

5. APPROACH OF THE WORK

5.1 Introduction

In this chapter, I will discuss how we proceeded with our task. The following flow chart gives a simple outlook about the approach of our work.



The first task was to prepare measurements. Preparing measurement means reading the measurement files in a format executable by our retrieval algorithm. The second phase of the work is the retrieval of the desired parameter i.e. the concentration of methane. The retrieval algorithm SFIT4 (v003.94) was used which is based on optimal estimation. In the refine retrieval part, the retrieval is refined using filters based on a statistical distribution called chi-square

distribution. The filtering was done to eliminate outliers and bad measurement points. And in the last part, the results are analyzed and compared to models.

5.2 Experimental setup

Section 5.2 is based on the paper Latitudinal variations of trace gas concentration by Notholt et al. , (2000)

The experiment has been performed using a Bruker 120M interferometer. The instrument was installed in a thermo stated laboratory container on the helicopter deck in the back of the ship, ten (10) meters above sea level. The solar tracker was placed on the container's roof. It was controlled by a 4-quadrant diode to follow the sun despite the ship movement. The solar tracker was adjusted to move faster than the ground-based measurement to overcome the ship movements. For reducing the influence of the ship rolling, the scanning arm of the interferometer had been installed parallel to ship's movement. Later, it was found that the pitching of the ship i.e. the up and down movements of the forepart of the deck and quarter deck was more dominant than rolling. Rolling was reduced by the stabilizer fin of the ship.

The interferometer and solar tracker worked satisfactorily for the wind velocities of around 15 ms^{-1} . Under stronger wind velocities, the motors of the solar tracker could no longer keep the image of the sun on the entrance aperture. More ever, under these wind condition, the spectra yielded erroneous interferograms, because the scanning mirror had to move up and down following the pitching. However, under strong wind conditions the measurements had to be stopped as due to the sea spray splashing against the mirror of the solar tracker.

The vibrations of the ship engines in the frequency range of 20-30 Hz were assumed to be the strongest disturbances on the interferometer. The stability of the interferometer has been tested using an artificial light source and studying the variability of the center burst during the alignment mode. The intensity in the IR varied by 1-2 % whereas in the UV the peak to peak intensity fluctuations increased up to 30 %. The alignment of the interferometer was checked daily by studying the interference fringes using an external HeNe-laser equipped with a

8cm diameter telescope to cover the whole beam area. After installation, the alignment was found to be stable during the whole cruise.

Spectra were recorded with an optical path difference (OPD) of 180 cm which corresponds to a unapodized resolution of 0.005cm^{-1} , using sun as the light source. In order to increase the signal-to-noise ratio, interference filters have been used to narrow the optical bandwidth. For a good latitudinal coverage, each spectral region was recorded in the morning, around noon and in the evening.

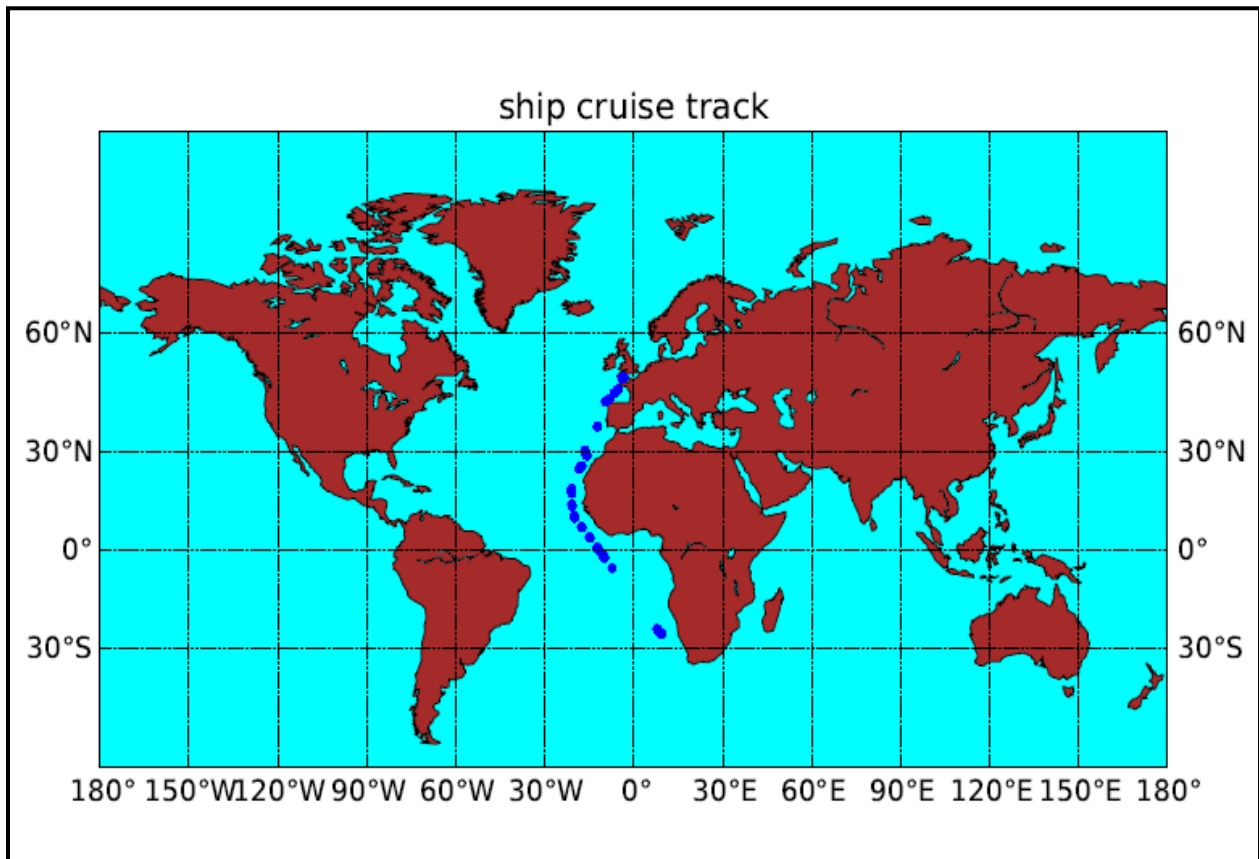


Figure 5.1: Map showing the location of the measurement points.

Figure 5.1 shows a map indicating the location of the measurement points. The measurements were taken between 48.8°N and 25.8°S .

5.3 CH₄ retrieval strategy via SFIT4

For analyzing our recorded spectra we used the SFIT4 retrieval algorithm (v003.94) which is a profile retrieval algorithm and based on optimal estimation. The strategy to retrieve methane with the SFIT4 algorithm is given below:

CH ₄ retrieval strategy via SFIT4(v003.94)			
Micro-windows [cm ⁻¹]	MW1: 2613.7-2615.40	MW2: 2835.50-2835.80	MW3: 2921.0-2921.60
Interfering Species	H ₂ O , HDO	HDO	H ₂ O , HDO , NO ₂
Regularization Constrain	First Order:Tikhonov		
Spectroscopic Line list	HITRAN 2008(Old line list)		
	Prelim project (New line list)		
A priori	WCCAM		

Table 5.1: CH₄ retrieval strategy via SFIT4

The common interfering gas in the three micro windows is water vapor (H₂O). HDO is also an isotope of water vapor. In our retrieval we used two different water vapor a priori profiles. We used the a priori profiles from the WCCAM (The Whole Atmosphere Community Climate Model) model and secondly we used the a priori water vapor profiles from the NCEP (National Centers for Environmental Predictions) . WCCAM assumes a standard atmosphere, where as in NCEP model data is assimilated with measurement. So, the a priori from the NCEP model is assumed to be more accurate and realistic than the WCCAM model. For the rest

of the interfering species the a priori profiles have been taken from the WCCAM model. The WCCAM profiles of the inferring species excluding water vapor are scaled during the retrieval process. Water vapor interference is accounted in a two step strategy. At first a dedicated H₂O retrieval is performed. Secondly, the retrieved daily mean H₂O profile is scaled in the subsequent CH₄ retrieval process.[*Sepulveda et al.*]

We have used two different databases for our spectroscopic parameters. First, we used the spectroscopic parameters from the HITRAN 2008 (*Rothman et al., 2009*) which we called the old line list. Secondly we use the spectroscopic parameters from the Prelim Project which we call the new line list. The Prelim project is a joint venture between the Institute of Environmental Physic (IUP), Karschule Institute of Technology (KIT) and German Aerospace Center (DLR). The spectral parameters in the old line is measured and calculated. On the other hand, the line parameters in the new line list are precisely measured where the spectral parameters are also resolved more accurately than the old line list. Therefore, we expect the performance of our retrieval with new line list better than the old line list.

5.4 Analysis Strategy

Our spectrometer measures the solar absorption with a high resolution Fourier Transform Spectrometer. These measured spectra are simulated with the help of a line by line radiative transfer code i.e. in our case SFIT4. The basic equation to analyze spectra is the Beer-Lambert's law:

$$I(\lambda) = I_{\text{sun}}(\lambda) \exp\left(-\int_{\text{TOA}}^{\text{obs}} \sigma_x(\lambda, s(\mathbf{T}, \mathbf{p})) \cdot x(s) ds\right) \quad (5.1)$$

Where ,

$I(\lambda)$ = measured intensity at wavelength λ

$x(s)$ = concentration of the absorber at the location s

I_{sun} = the extraterrestrial solar intensity

σ_x = absorption cross-section of the absorber

The integration range is between the observer and the top of the atmosphere. [Sepulveda et al.]. Our target is to find $x(s)$ from the measured solar intensity $I(\lambda)$. So for the numerical analysis, the atmospheric state $x(s)$ is discretized in a form of state vector x and the measured solar intensity $I(\lambda)$ is discretized in the form of measurement vector y . The state and the measurement vector are related with a vector valued function F , where F simulates the atmospheric radiative transfer and the characteristics of the measurement system i.e. spectral resolution, instrumental line shape etc. [Sepulveda et al.].

$$y = F(x) + \varepsilon \quad (5.2)$$

Based on the analysis as discussed in chapter 3 section 3.4 (Linear problem with measurement error) the solution of equation (5.2):

$$\hat{x} = x_a + S_a K^T (K S_a K^T + S_\varepsilon)^{-1} (y - K x_a)$$

5.5 Total column to column average dry-air-mole fraction

The analysis of the solar absorption gives us the total column of methane. We convert the total column to column averaged dry -air -mole fraction. Dry-air-mole fractions are independent of solar zenith angle, surface pressure and humidity. Therefore dry-air-mole-fractions are more useful tracers of source and sink processes.

$$X_i = \frac{VC_i}{\frac{P_s}{m_{air}^{dry}} - VC_{H_2O} \frac{m_{H_2O}}{m_{air}^{dry}}} \quad (5.3)$$

[Deutscher et al. , 2010]

Where,

X_i = Column averaged dry-air-mole fraction of gas i (ppbv/ppm/ppt)

VC_i = Vertical column of gas i (molecules cm^{-2})

P_s = Surface pressure (mb)

$m_{\text{air}}^{\text{dry}}$ = molecular mass of dry air 28.964 gmol^{-1}

$m_{\text{H}_2\text{O}}$ = molecular mass of dry water 18.02 gmol^{-1}

$g(\Phi)$ = Latitude dependent gravitational acceleration (ms^{-2})

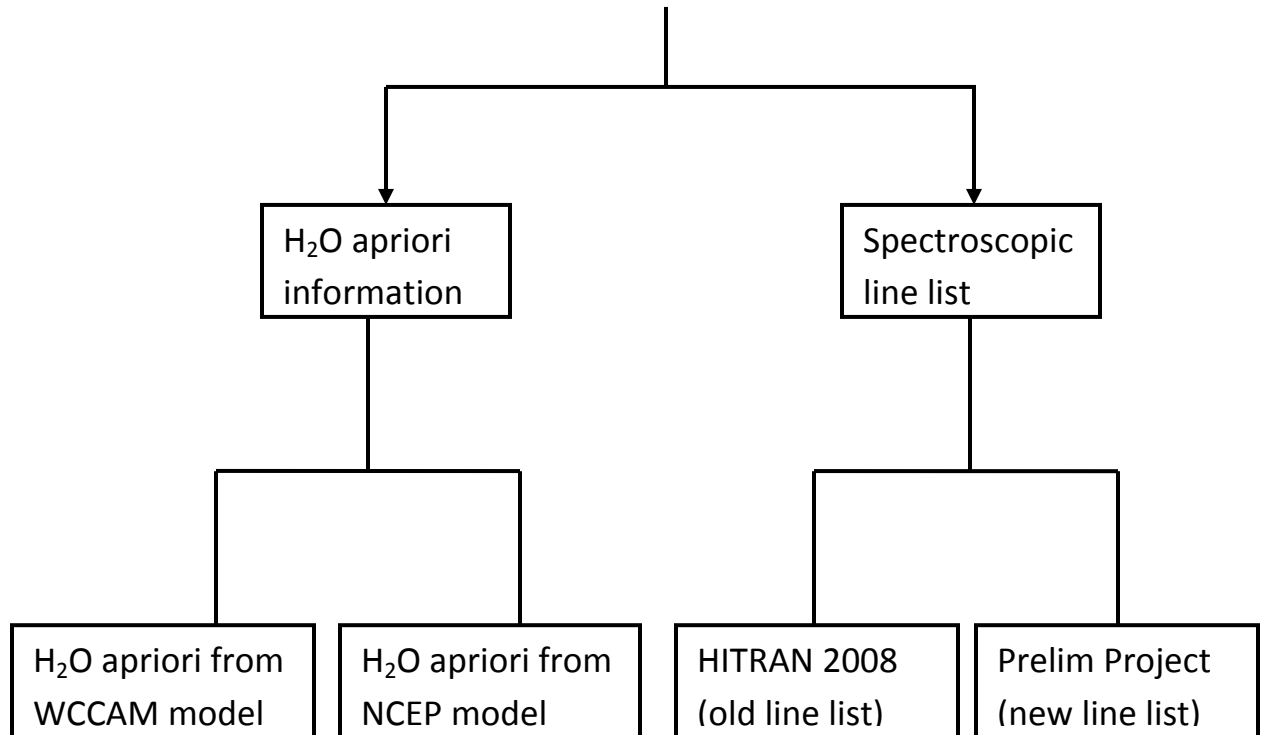
6. DATA ANALYSIS

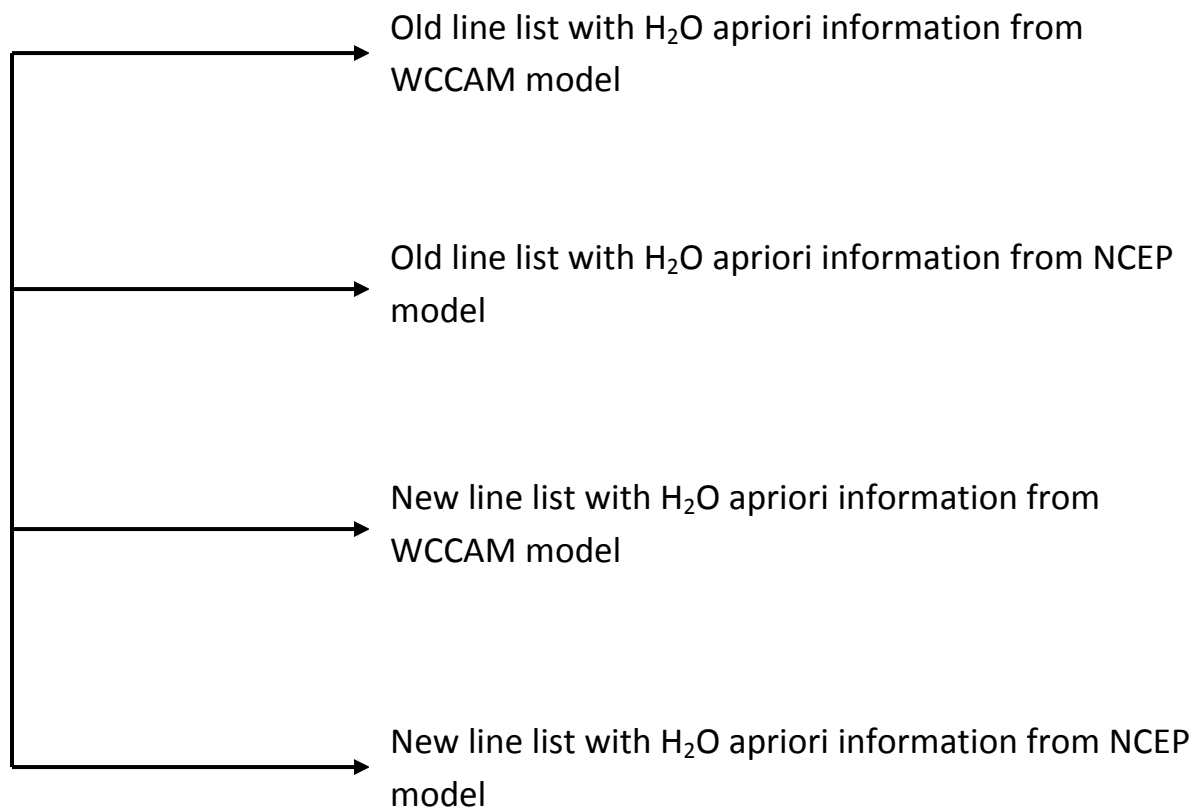
6.1 Preparing measurements

The measurements were saved in house-keeping files called run log files. The measurements were read from the run log files and written in a fixed format manner in an executable format called the sun run file. Another sun run file was created containing the date of the measurements, latitude and longitude of the measurement points. This sun run file was the input to the retrieval algorithm along with pressure and temperature data.

6.2 Retrieval

Methane is retrieved in four different manners depending on the spectral line lists and H₂O a priori information. The four different types are:





6.2.1 Retrieval with old line lists

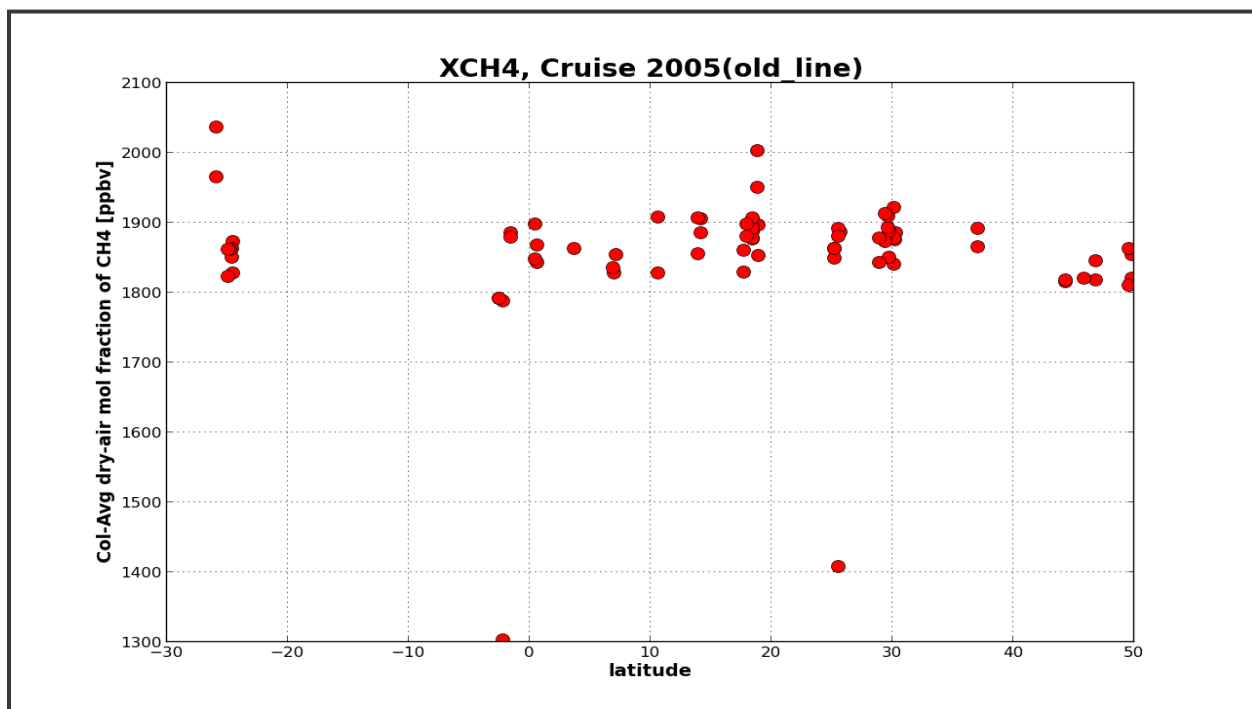


Figure 6.1: Retrieval of methane using the old line list and H₂O apriori from WCCAM model

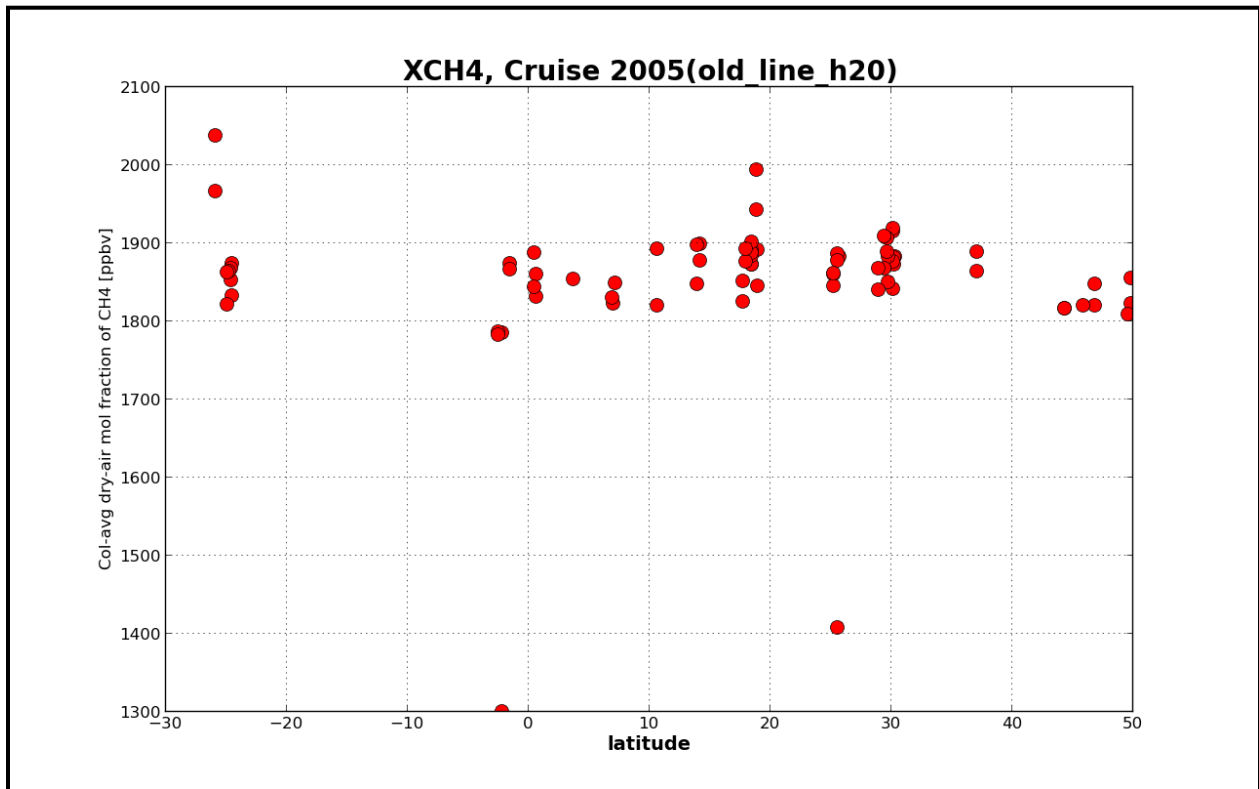


Figure 6.2: Retrieval of methane using the old line list and H₂O apriori from NCEP model

Figure 6.1 shows the retrieval of methane using the old line list and water vapor apriori from the WCCAM model. Multiple points at each latitudes show the multiple measurements at particular latitude. Similarly, figure 6.2 shows the retrieval of methane using the old line list and water vapor apriori from the NCEP model. To interpret the plots, daily means of the measurements are taken. That means the measurements of a particular day are averaged at particular latitude.

Figure 6.3 and 6.4 show the daily mean column average dry-air mole fraction of methane using the old line list. The average concentration of methane retrieved using the old line list and water vapor apriori from the WCCAM model is 1855 ± 11 ppbv . Average concentration of retrieved methane using the old line

list and water vapor apriori from the NCEP model is 1852 ± 11 ppbv. Using two different water vapor apriori seems not to effect the retrieval to a large extent.

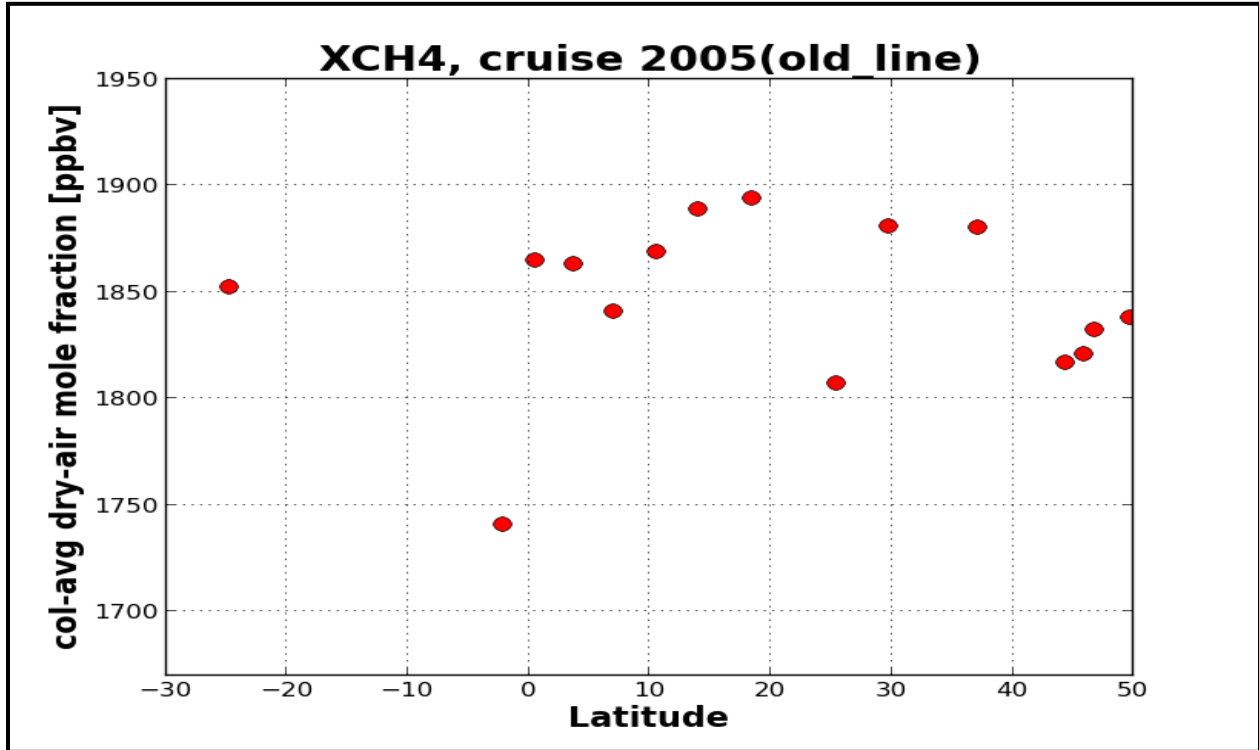


Figure 6.3: Retrieval of methane using the old line list and H₂O apriori from NCEP model

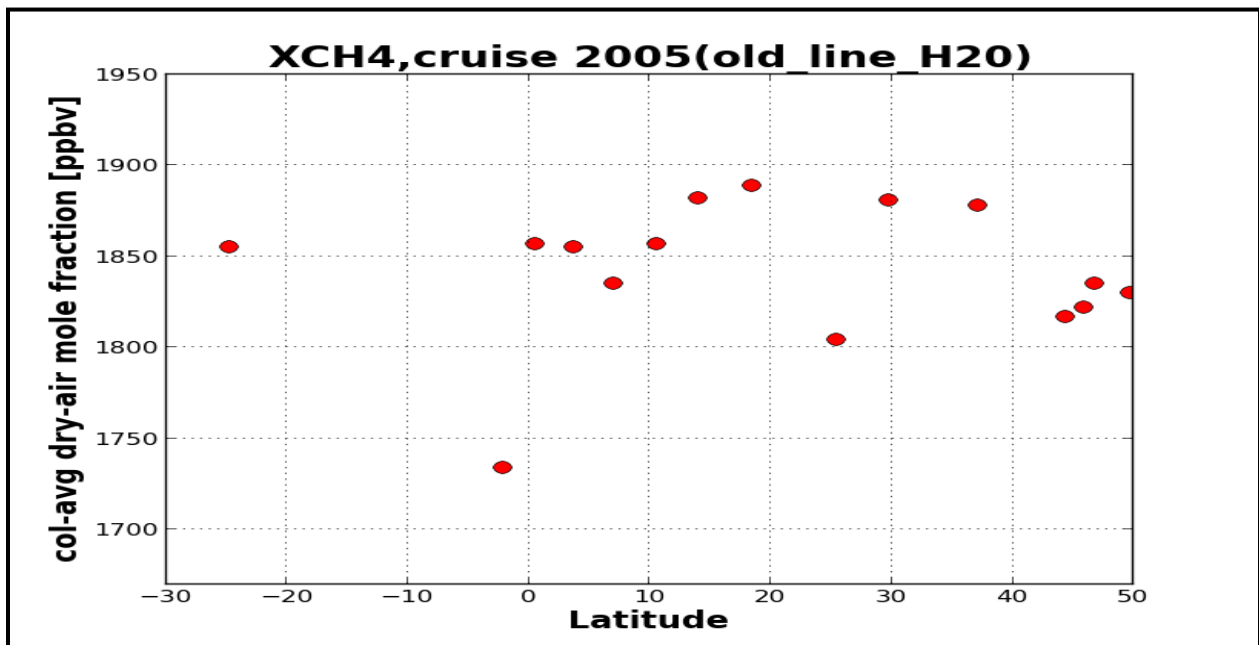


Figure 6.4: Retrieval of methane using the old line list and H₂O apriori from NCEP model

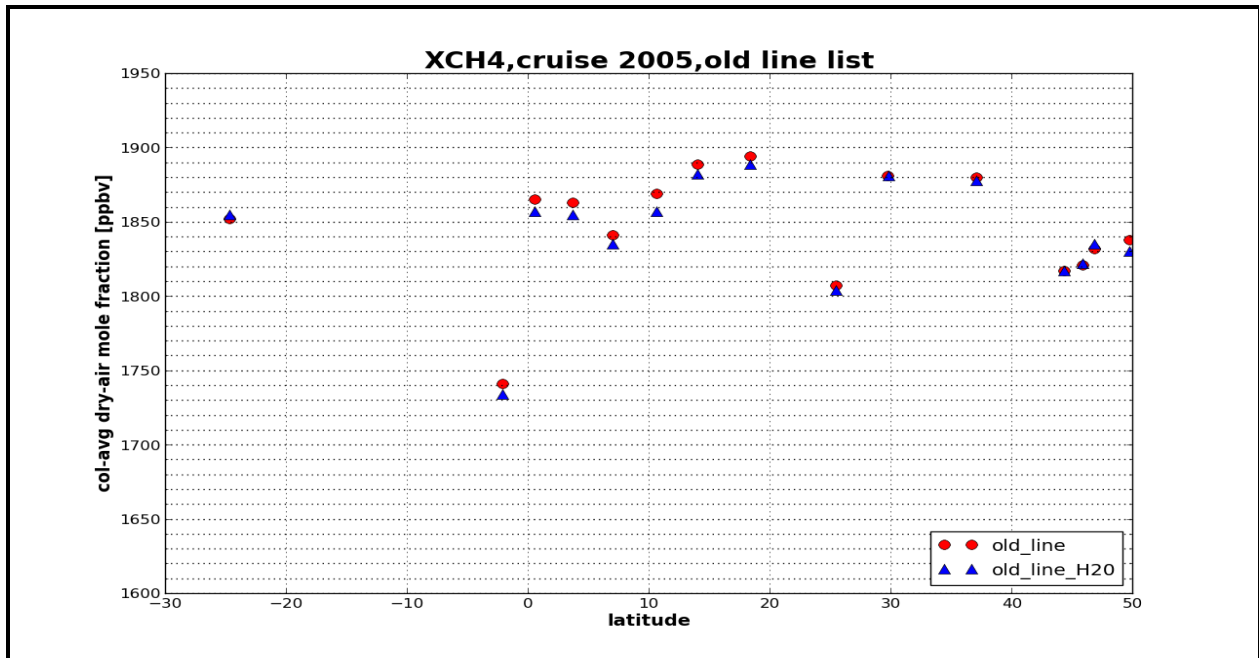


Figure 6.5: (1) Red curve: Old line list and H₂O apriori from WCCAM. (2) Blue curve: Old line list and H₂O apriori from NCEP

6.2.2 Retrieval with new line lists

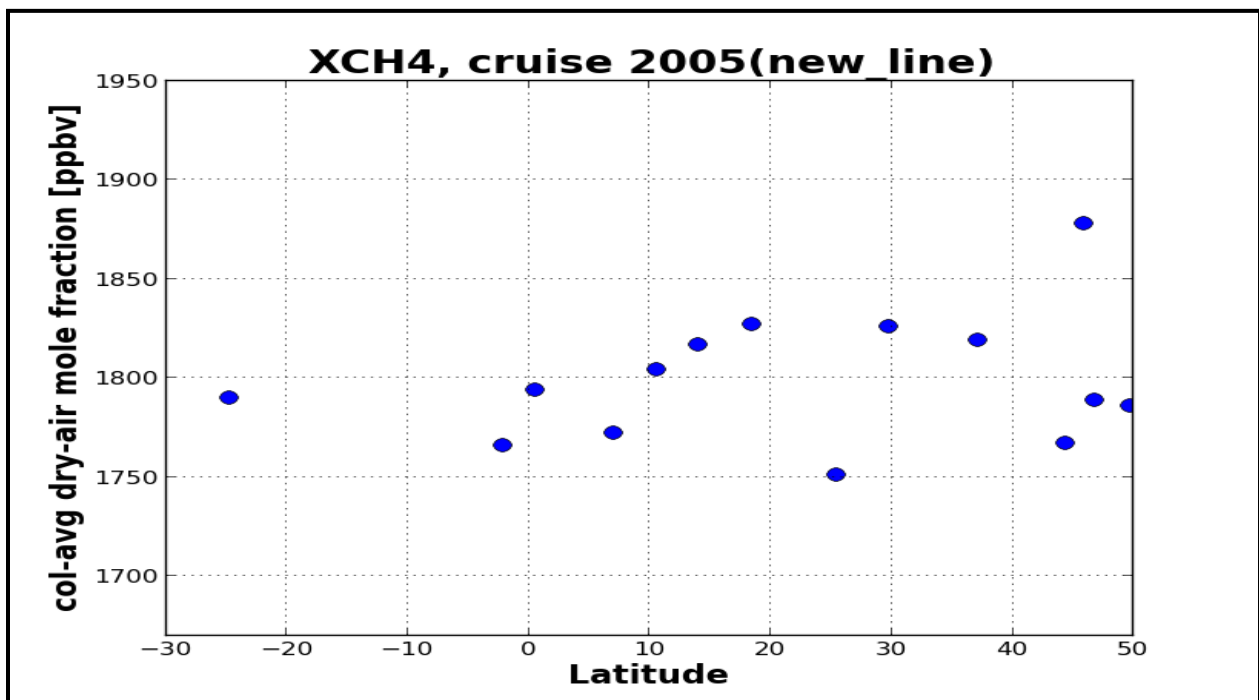


Figure 6.6: Retrieval of methane using the new line list and H₂O apriori from WCCAM model

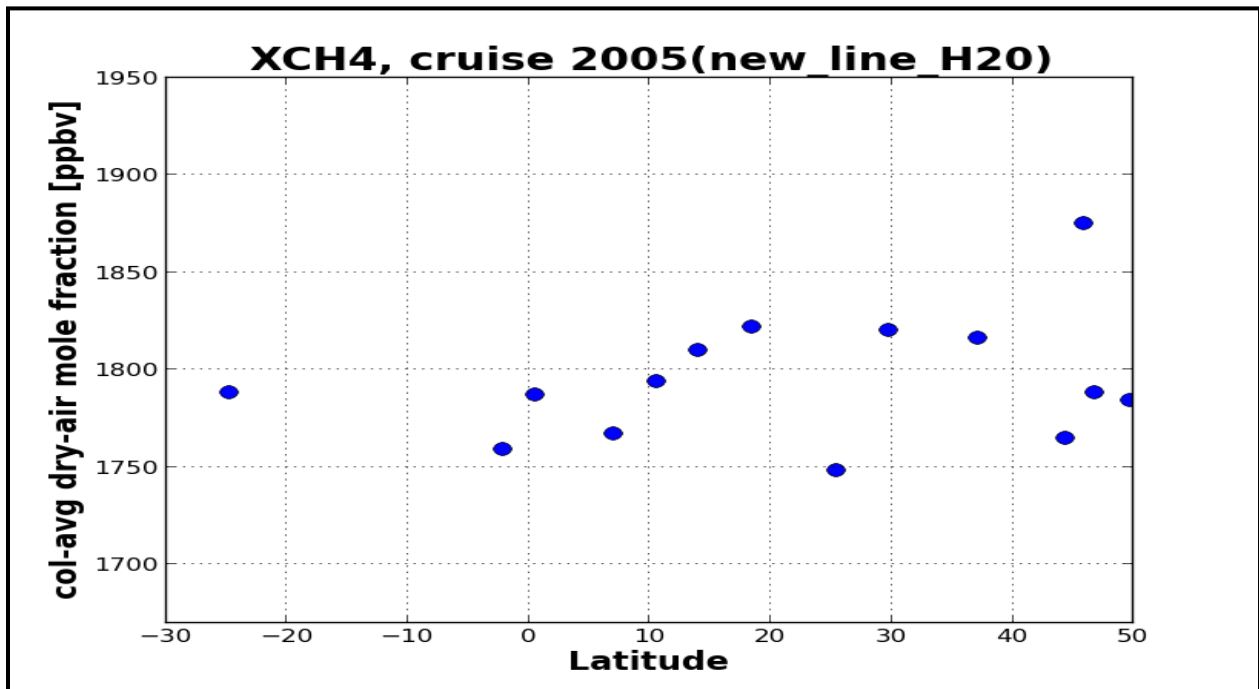


Figure 6.7: Retrieval of methane using the new line list and H₂O apriori from NCEP model

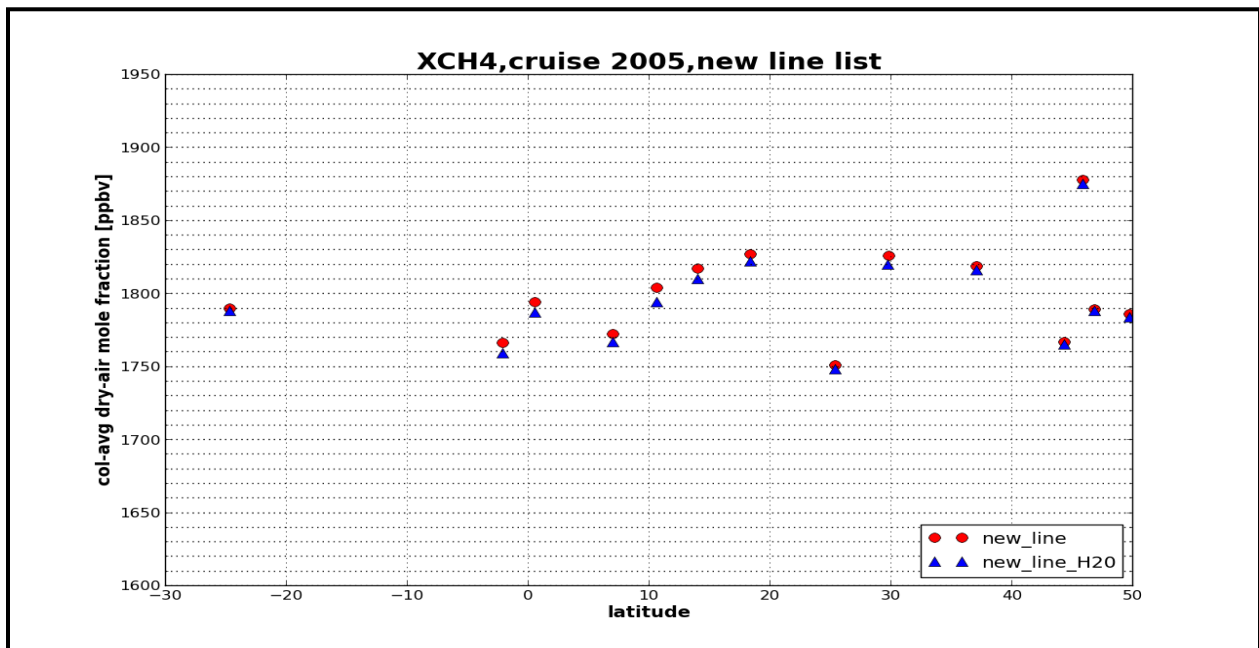


Figure 6.8: (1) Red curve: New line list and H₂O apriori from WCCAM. (2) Blue curve: New line list and H₂O apriori from NCEP

Figure 6.6 and 6.7 show the retrieved methane concentration using the new line list. Retrieval using the new list shows lower concentration of methane compared to the retrieval using the old line list. As stated previously, the spectroscopic parameters in the new line list are resolved more precisely than the old line list. The interference of the absorbing species in the retrieval using the new line is reduced more efficiently compared to the retrieval using the old line list. Hence, methane concentration is lower in the retrieval using the new line list. The average concentration of methane retrieved using the new line list and water vapor a priori from the WCCAM model is 1783 ± 12 ppbv. Average concentration of retrieved methane using the new line list and water vapor a priori from the NCEP model is 1778 ± 12 ppbv.

6.2.3 Comparison between retrieval with old and line lists

To compare the retrievals the residuals of the measurements are examined. Figure 6.9 – 6.12 show the residuals of the same measurement point. Residuals show the difference between our observed and calculated spectra. The residuals of the retrieval with old line lists show higher difference between the observed and calculated spectra compared to the residuals of the retrieval with new line list. The retrieval algorithm is based on the fitting of an observed spectrum to a simulated spectrum. The simulated spectrum is calculated based on the a priori state of the atmosphere, spectral parameters and other influences such as instrumental influences. As, the spectral parameters in the new line list are more precisely resolved than the old line list, the fit between the measured and calculated spectra using the new line list is better than the old line list. Therefore, the residuals of the retrieval using the new line list show lower difference. This yields the improvement of the retrieval using the new line list.

To account for the effect of using two different water vapor a priori the residuals of the retrieval using similar line list but different water vapor a priori information is compared.

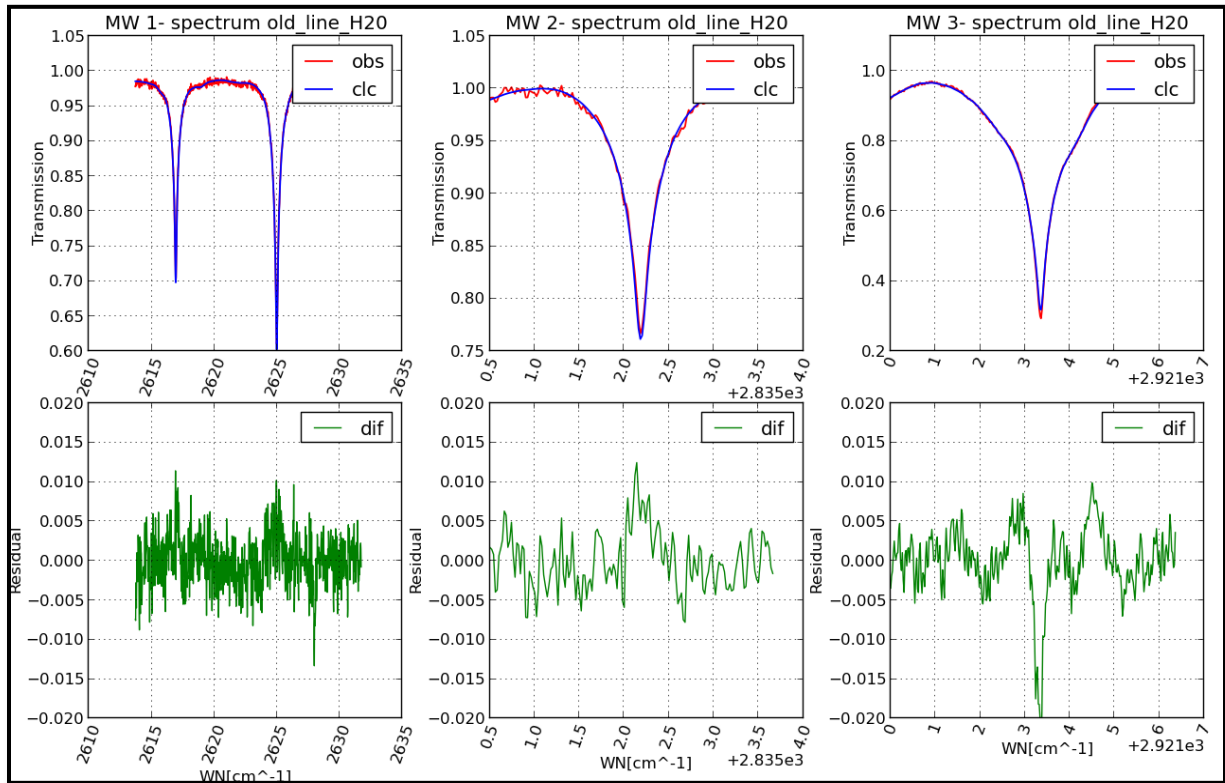


Figure 6.9: Residuals of measurement retrieved with old line list and H₂O apriori from NCEP model

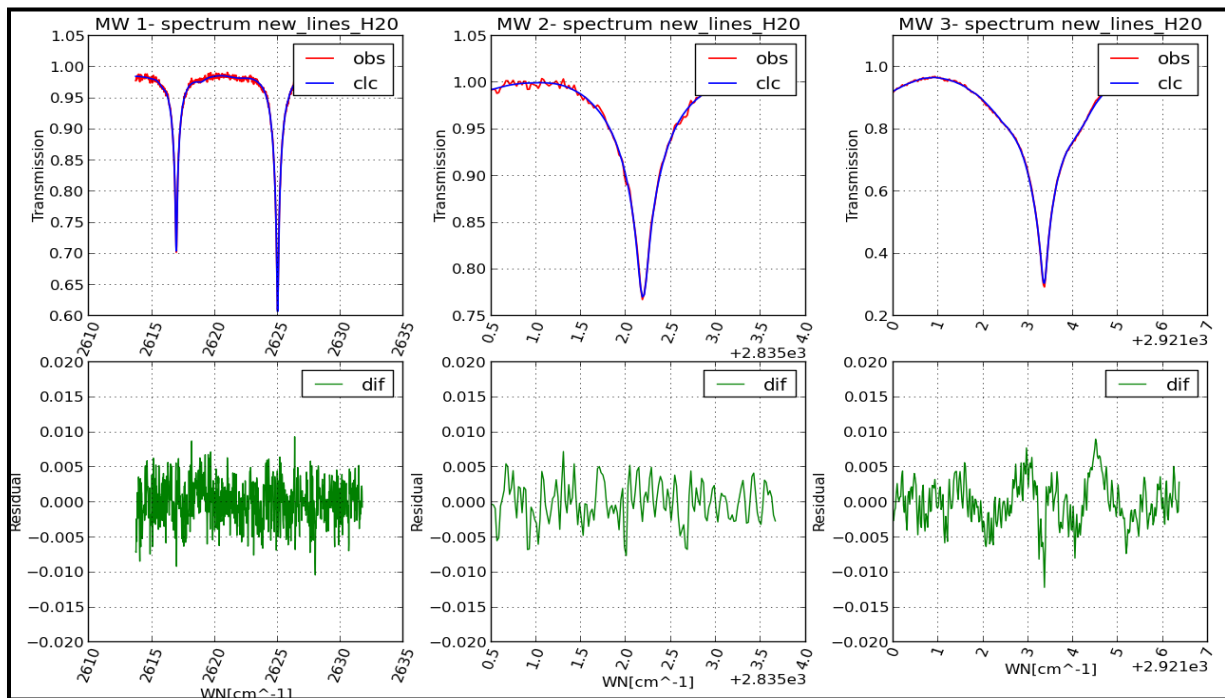


Figure 6.10: Residuals of measurement retrieved with new line list and H₂O apriori from NCEP model

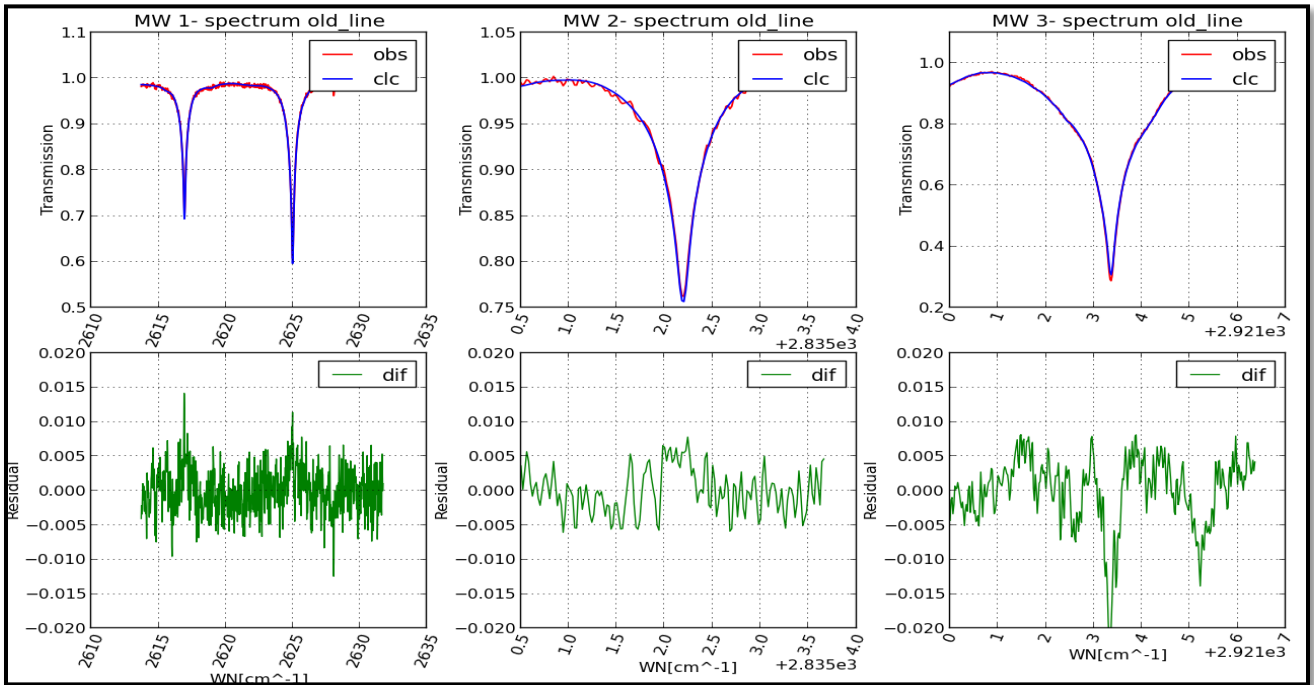


Figure 6.11: Residuals of measurement retrieved with old line list and H₂O apriori from WCCAM model

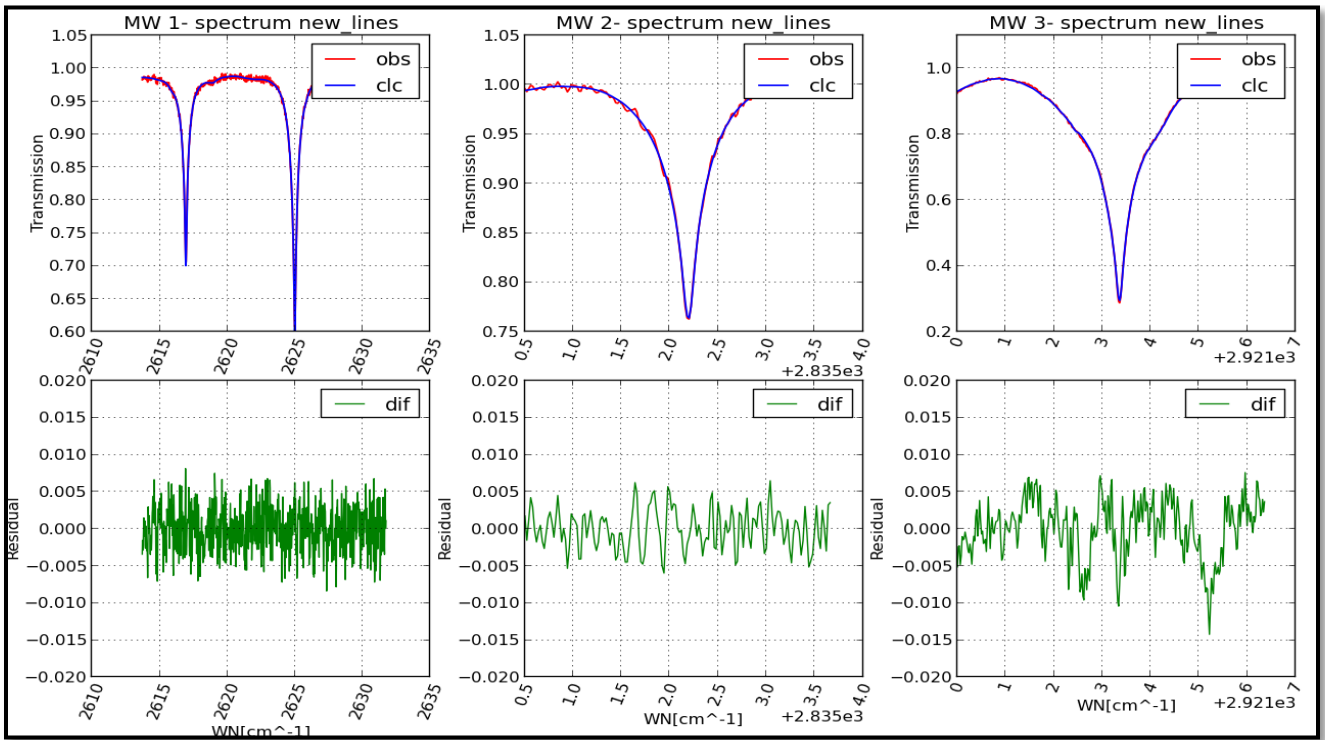


Figure 6.12: Residuals of measurement retrieved with new line list and H₂O apriori from WCCAM model

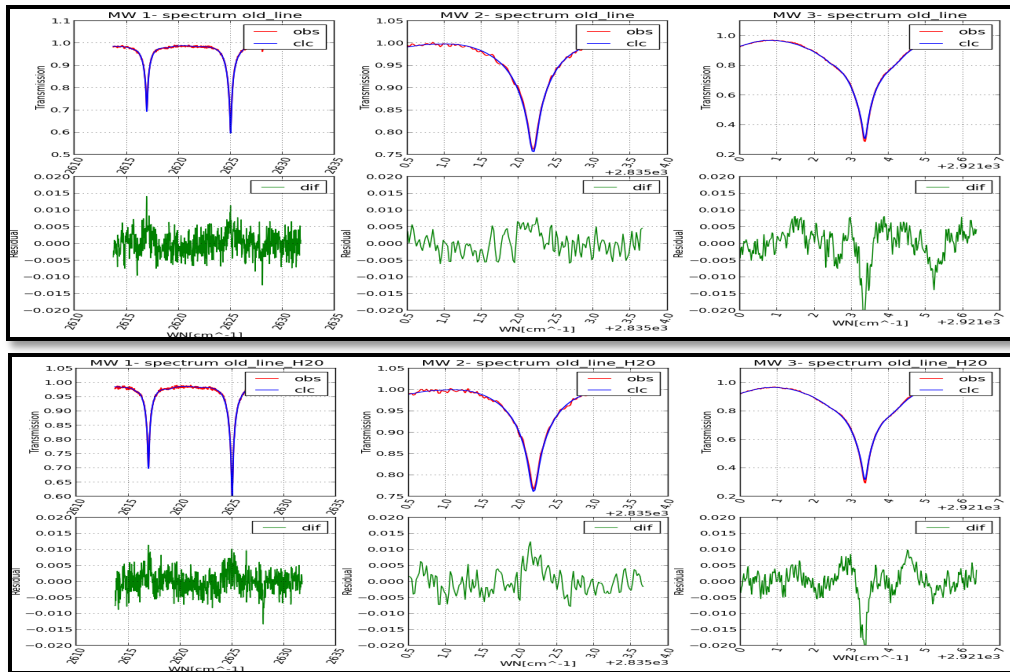


Figure 6.13: Comparison between residuals of retrieval using old line list and different water vapor apriori information

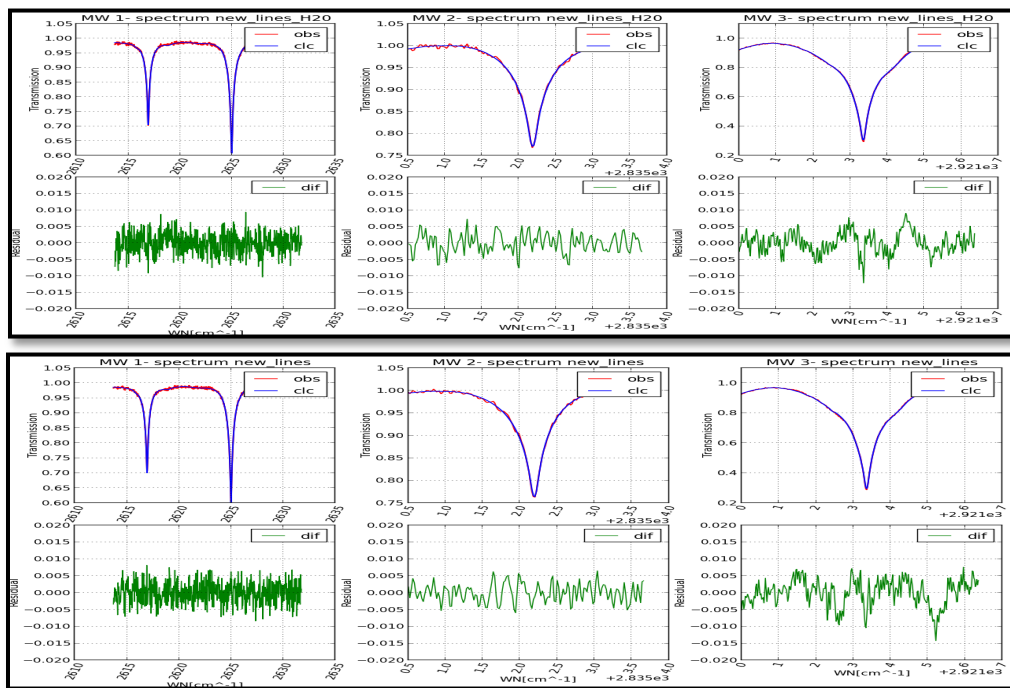


Figure 6.14: Comparison between residuals of retrieval using new line list and different water vapor apriori information

Retrieval using the water vapor apriori information from the NCEP model shows less variation in the residuals for both the line list. The apriori from the NCEP model is assimilated with measurement which is more accurate than the WCCAM model data. Hence, the retrieval of water vapor based on the apriori from the NCEP model gives us a better retrieval of water vapor. As water vapor is scaled to the methane retrieval, the better water vapor retrieval improves the minimization of water vapor interference in the target gas retrieval and therefore showing lower variation in the residuals.

6.2.4 Chi-square value

To select the best retrieval a statistical parameter called chi-square value is used. Chi-square is a special Gaussian distribution with zero mean and unit variance. If a random variable is defined as:

$$\chi^2 = \sum_{i=1}^u x_i^2$$

[Menke, 1989]

Then the random variable is said to have a chi-square (χ^2) distribution with degrees of freedom u . To select the best retrieval the goodness of the fit of each retrieval is compared. The chi-square test is a way of testing whether a random variable belongs to a given Gaussian distribution. The chi-square test asks the question: 'what fraction of members of the Gaussian distribution has a probability density less than or greater than that of the vector being tested?' *[Rodgers, 2000]*. If the fraction f is smaller than the vector is described as 'significant at the 100 $f\%$ level'. *[Rodgers, 2000]*. That means low chi-square value indicates the goodness of our fit. To be more specific, lower chi-square value means the difference between our observed and calculated value is low. Hence the fit is good. The average chi-square values of the four different type of retrieval are given in the table below:

Retrieval	Average chi-square value
Old line list and water vapor apriori from the WCCAM model	4.166
Old line list and water vapor apriori from the NCEP model	4.066
New line list and water vapor apriori from the WCCAM model	2.471
New line list and water vapor apriori from the NCEP model	2.464

Table 6.1: Average chi-square values of different retrieval

The average chi-square values for retrievals using the new line list are almost half the values of the retrieval using the old line list. This shows the improvement of the retrieval using the new line list as it was seen examining the residuals of the retrieval. From the average chi-square values it is evident that, the retrieval using the new line list and water vapor apriori from the NCEP model is the best retrieval among the four retrievals. The effect of using two different apriori information is also noticeable from the chi-square values. For the old line list retrieval, the difference of using two different water vapor apriori is $\sim 10\%$. Whereas, using two different water vapor apriori information for the new line list accounts a difference of $\sim 0.7\%$. The different water vapor apriori information has higher impact on the retrievals using the old line list. Retrievals using the new line list are almost independent of the water vapor apriori information used. This remarks the better quality of the retrieval with new list compared to the old line list.

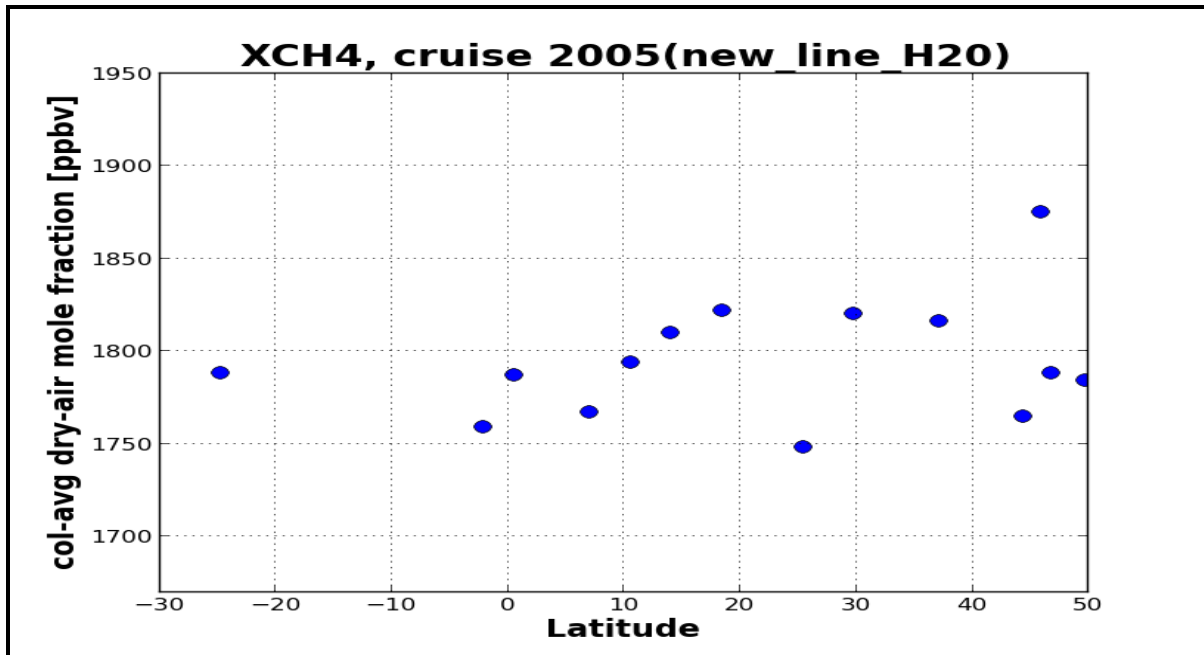


Figure 6.15: Retrieval of methane using new line list and H₂O apriori from NCEP model (best retrieval)

6.3 Refine retrieval

The retrieved methane concentration needs to be refined to remove outliers and bad measurements. Bad measurements mean a measurement having high and unsymmetrical variation in the residuals i.e. the fit between the observed and calculated spectra is not good. Figure 6.16 shows an example of such bad measurement. For refining the retrieval a statistical parameter chi-square critical value is used. The critical value of a chi-square value is defined as, a value compared to which one can determine whether a possible outcome is likely or unlikely. Figure 6.17 shows a standard chi-square distribution table. The red blocked numbers are the critical values of a chi-square distribution for a specified degree of freedom. If a chi-square value for a specified degree of freedom is higher than the critical value than the possible outcome of an event is unlikely. Similarly, if the chi-square value for a specified degree of freedom is lower than the critical value and lies in between the 5% and 95% mark, then the possible outcome of the event is said to be likely.

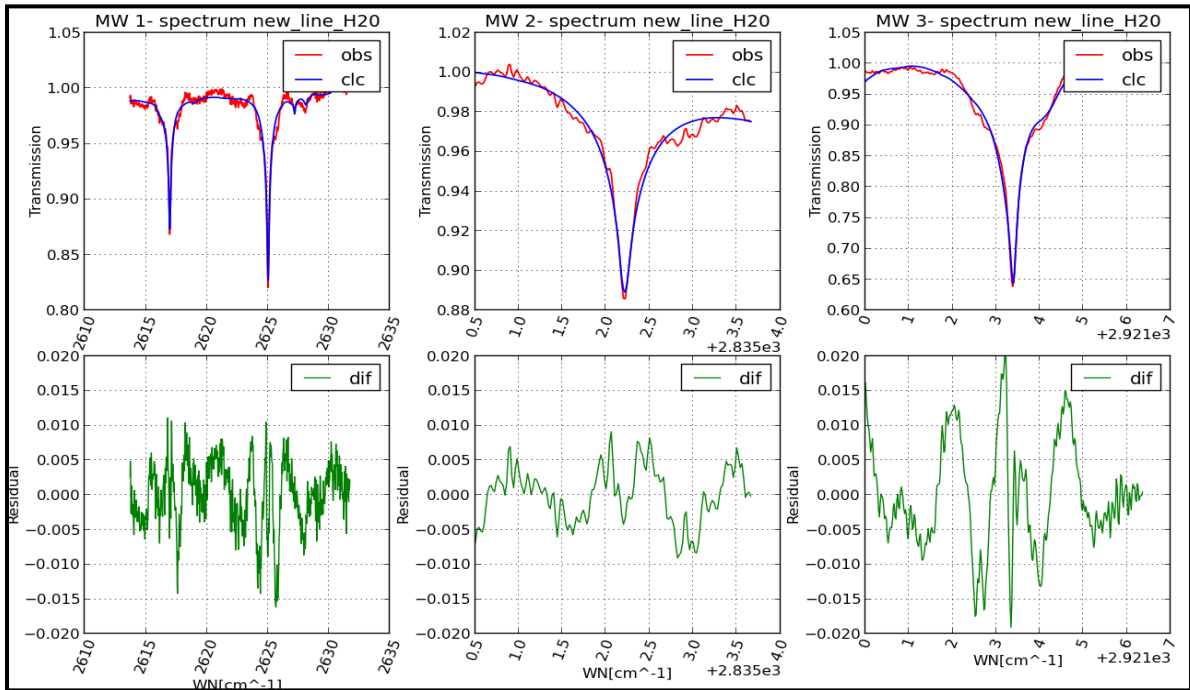


Figure 6.16: Example of a bad measurement

Percentage Points of the Chi-Square Distribution									
Degrees of Freedom	Probability of a larger value of χ^2								
	0.99	0.95	0.90	0.75	0.50	0.25	0.10	0.05	0.01
1	0.000	0.004	0.016	0.102	0.455	1.32	2.71	3.84	6.63
2	0.020	0.103	0.211	0.575	1.386	2.77	4.61	5.99	9.21
3	0.115	0.352	0.584	1.212	2.366	4.11	6.25	7.81	11.34
4	0.297	0.711	1.064	1.923	3.357	5.39	7.78	9.49	13.28
5	0.554	1.145	1.610	2.675	4.351	6.63	9.24	11.07	15.09
6	0.872	1.635	2.204	3.455	5.348	7.84	10.64	12.59	16.81
7	1.239	2.167	2.833	4.255	6.346	9.04	12.02	14.07	18.48
8	1.647	2.733	3.490	5.071	7.344	10.22	13.36	15.51	20.09
9	2.088	3.325	4.168	5.899	8.343	11.39	14.68	16.92	21.67
10	2.558	3.940	4.865	6.737	9.342	12.55	15.99	18.31	23.21
11	3.053	4.575	5.578	7.584	10.341	13.70	17.28	19.68	24.72
12	3.571	5.226	6.304	8.438	11.340	14.85	18.55	21.03	26.22
13	4.107	5.892	7.042	9.299	12.340	15.98	19.81	22.36	27.69
14	4.660	6.571	7.790	10.165	13.339	17.12	21.06	23.68	29.14
15	5.229	7.261	8.547	11.037	14.339	18.25	22.31	25.00	30.58
16	5.812	7.962	9.312	11.912	15.338	19.37	23.54	26.30	32.00
17	6.408	8.672	10.085	12.792	16.338	20.49	24.77	27.59	33.41
18	7.015	9.390	10.865	13.675	17.338	21.60	25.99	28.87	34.80
19	7.633	10.117	11.651	14.562	18.338	22.72	27.20	30.14	36.19
20	8.260	10.851	12.443	15.452	19.337	23.83	28.41	31.41	37.57
22	9.542	12.338	14.041	17.240	21.337	26.04	30.81	33.92	40.29
24	10.856	13.848	15.659	19.037	23.337	28.24	33.20	36.42	42.98
26	12.198	15.379	17.292	20.843	25.336	30.43	35.56	38.89	45.64
28	13.565	16.928	18.939	22.657	27.336	32.62	37.92	41.34	48.28
30	14.953	18.493	20.599	24.478	29.336	34.80	40.26	43.77	50.89
40	22.164	26.509	29.051	33.660	39.335	45.62	51.80	55.76	63.69
50	27.707	34.764	37.689	42.942	49.335	56.33	63.17	67.50	76.15
60	37.485	43.188	46.459	52.294	59.335	66.98	74.40	79.08	88.38

Figure 6.17: Standard chi-square distribution table [Downloaded from whichbobareyou.com/links-and-stuff.html on 25/07/2013]

The possible outcome of the retrieval is whether the fit between the expected and calculated spectra is good or bad. So, the degree of freedom for the chi-square distribution of the retrieval is one (1). From the standard chi-square distribution table, the critical value for a chi-square distribution with degree of freedom 1 is 3.84. That means, retrieved points having a chi-square value higher than 3.84 are unlikely. So, a chi-square filter of 3.84 can be used to filter out the bad and unlikely data points. To refine the retrieval two chi-square filters of 3.5 and 3.0 were used. The reason of using chi-square filters less than the critical value was not to stay on the boundary of the critical value. Two filters were used to examine the effect the two filters on the retrieval i.e. to find out which chi-square filter refines the retrieval better.

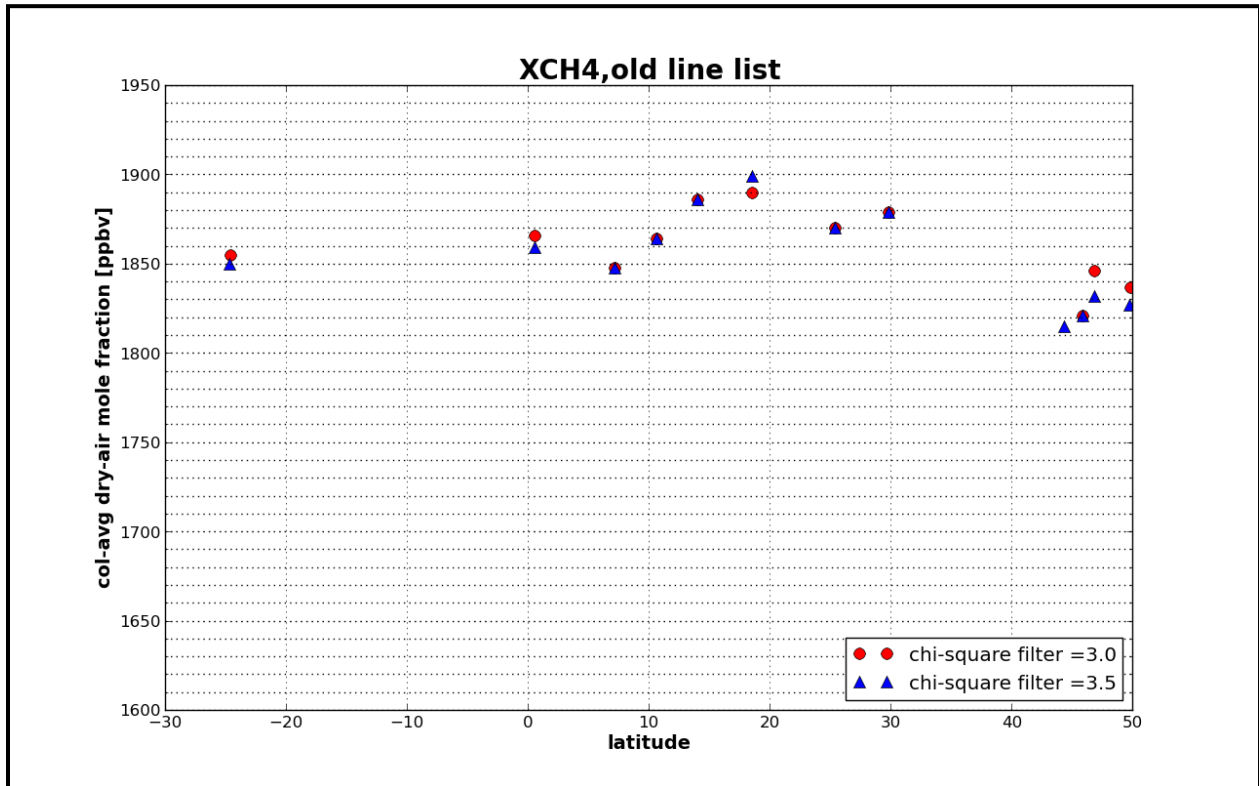


Figure 6.18: Refine of retrieval using old line list and H₂O apriori from WCCAM model

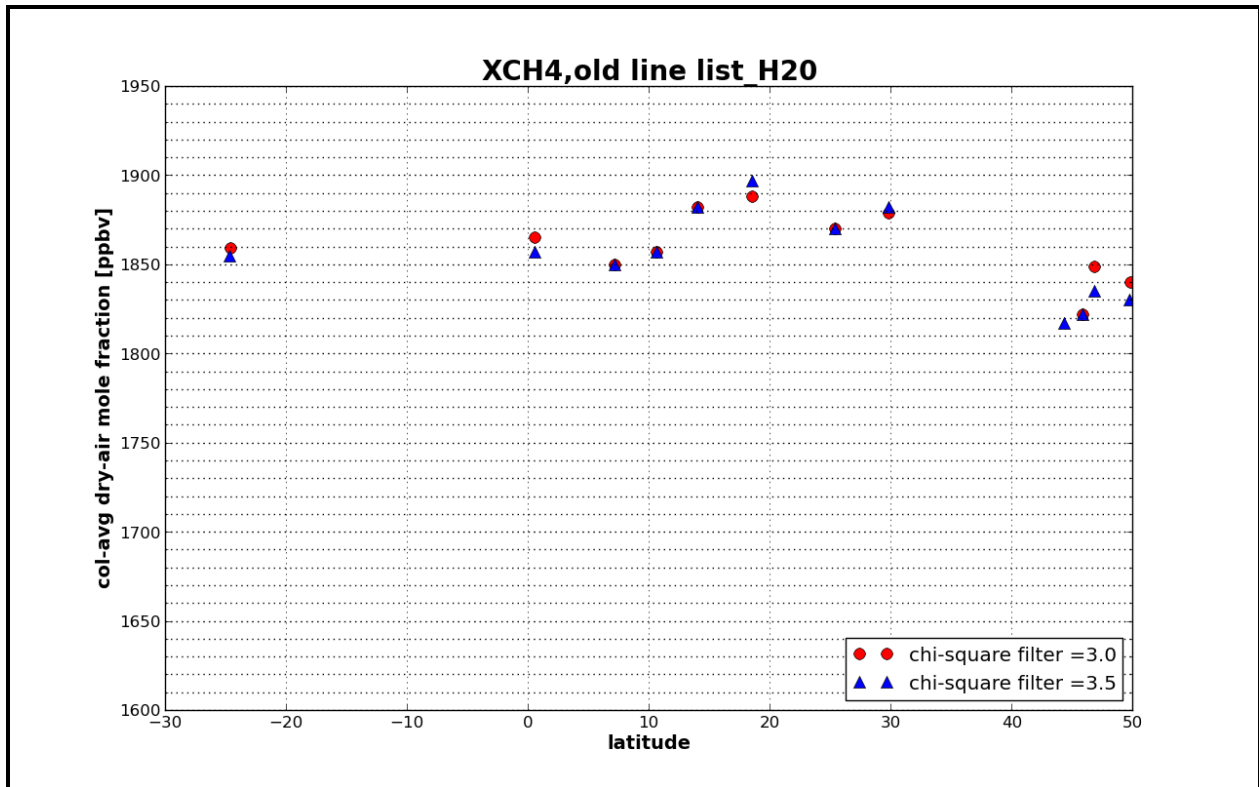


Figure 6.19 : Refine of retrieval using old line list and H₂O apriori from NCEP model

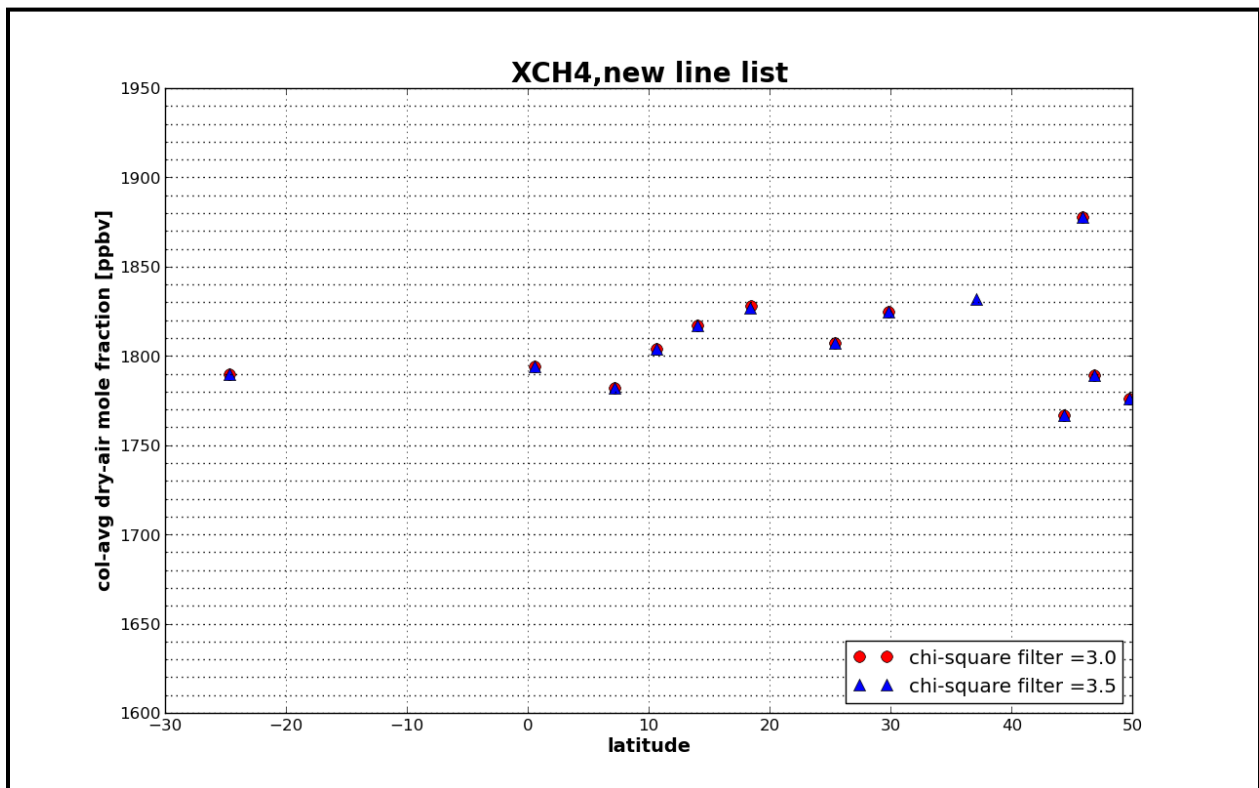


Figure 6.20: Refine of retrieval using new line list and H₂O apriori from WCCAM model

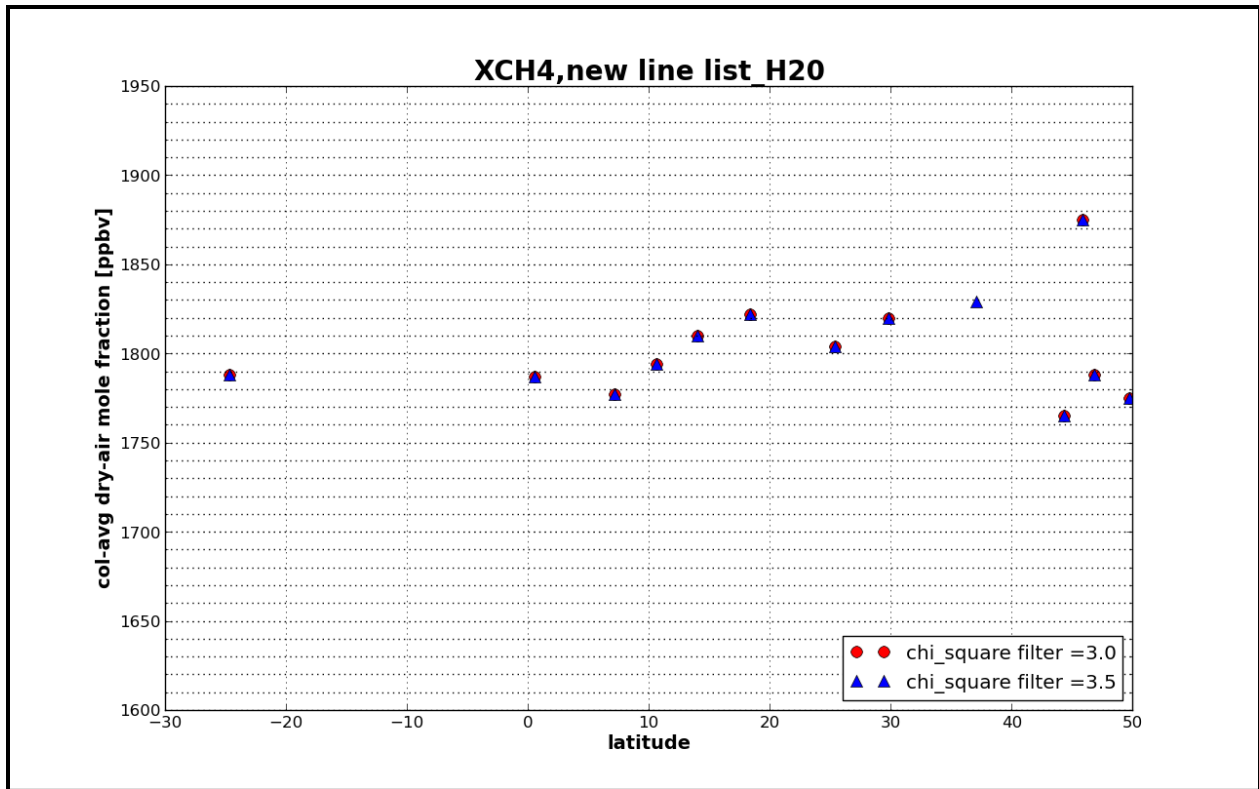


Figure 6.21: Refine of retrieval using new line list and H₂O apriori from NCEP model

Table 6.2 summarizes the effect of the chi-square filters on the retrievals. As seen from the table, the number of data points reduces after using the filters and the reduction rate of data points is higher for the chi-square filter 3.0. This yields, the lower the value of the chi-square filter the more efficient is the filtering and the retrieval is better refined. Moreover, the loss of data point is higher for the old list retrievals. This means the fit quality of retrieval based on new line list is better than the retrieval based on old line list. The average chi-square values for the retrieval using the new line lists are almost equal after filtering. This again proves retrievals using the new line list are almost independent of the water vapor apriori used. Retrieval based on new line list and water apriori from NCEP model

		Old line list and H ₂ O apriori from WCCAM model	Old line list and H ₂ O apriori from NCEP model	New line list and H ₂ O apriori from WCCAM model	New line list and H ₂ O apriori from NCEP model
Chi-square filter of 3.5	Total number of measurements	74	75	77	77
	Average chi-square value	4.164	4..066	2.471	2.464
	Number of data point after chi-square filter	57	60	65	64
	Average chi-square value	2.377	2.38	1.89	1.89
	Number of daily mean data points	13	13	13	13
	Average chi-square value	2.42	2.418	2.13	2.12
Chi-square filter of 3.0	Total number of measurements	74	75	77	77
	Average chi-square value	4.164	4..066	2.471	2.464
	Number of data point after chi-square filter	47	48	63	63
	Average chi-square value	2.184	2.16	1.85	1.86
	Number of daily mean data points	12	12	12	12
	Average chi-square value	2.21	2.19	2.03	2.03

Table 6.2: Summary of the effect of chi-square filters on the retrieval

has the lowest chi-square value for both the chi-square filter. For the chi-square filter of 3.0 it has a value of 2.03 which is lower than the value for chi-square value of 3.5. The number of daily mean data points is also less for the chi-square filter of 3.0. For the purpose of good interpretation it is not good to have too less data points. So, for a tradeoff between the chi-square value and the number of daily mean data point, the chi-square filter of 3.5 is chosen. For a chi-square filter of 3.5 the average chi square value for the retrieval based on new line list and water vapor apriori from the NCEP model is 2.12 and the number of daily mean data point is 13.

6.4 Interpretation of results

The concentration of methane is higher in the northern hemisphere compared to southern hemisphere. According to the WMO assessment [WMO, 1995], the atmospheric methane concentration in the northern hemisphere are on average about 6% higher than the southern hemisphere. [Notholt, 2000]. This is due to the source strength of methane in the northern hemisphere compared to the southern hemisphere. The average concentration of methane analyzed during the cruise 2005 is 1802 ± 6 ppbv. This concentration of methane is higher compared to the cruise data analysis in 2003 by Warneke et.al. (2006). In a study by Petersen et.al. , (2010), also showed enhanced methane concentration in the tropics during a measurement campaign in 2005. The study reveals higher influence of biomass burning sources in the tropics in 2005 compared to measurement campaign in 2004 and 2006. The mean concentration of methane calculated from the measurement campaign in 2005 was 1790 ± 10 ppbv whereas from cruise 2005 the calculated mean concentration of methane is 1802 ± 6 ppbv . Biomass burning i.e. natural burning of grassland or deforestation leads to high level of tropospheric trace gases, especially in the tropics. And the maximum intensity is found typically during October-November. [Notholt, 2000]. The strongest latitudinal gradient of methane observed in the Inter Tropical Convergence Zone [ICTZ]. On October 2005 the position of ICTZ was around 12.8° N.

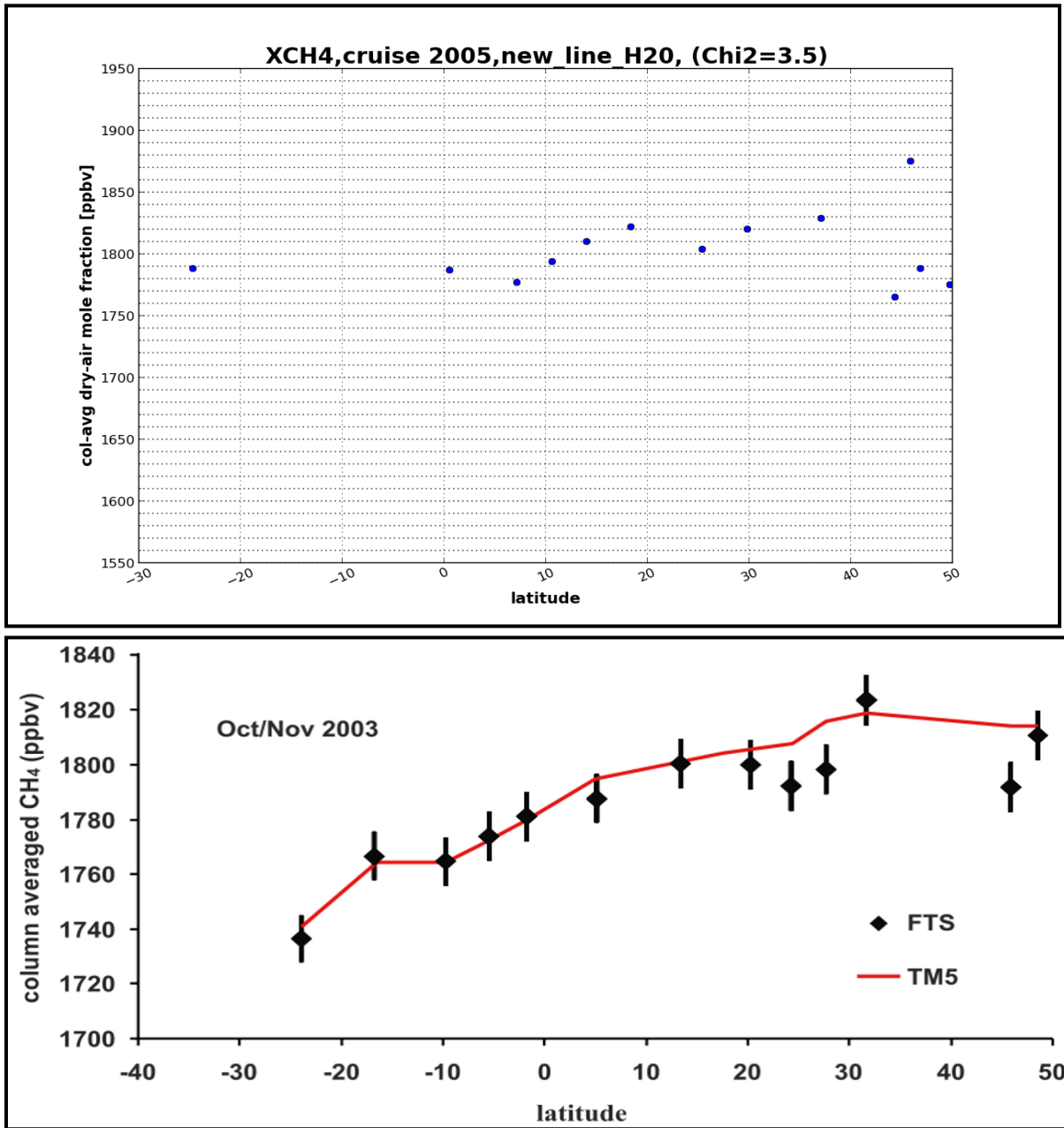


Figure 6.22: Comparison of cruise analysis of 2005 and 2003. Analysis of cruise 2003 is from Warneke et al.(2006)

6.5 Model Comparison

The retrieval results were compared with model results. The model data from the two-way nested global chemistry-transport zoom model TM5 were used for comparison.

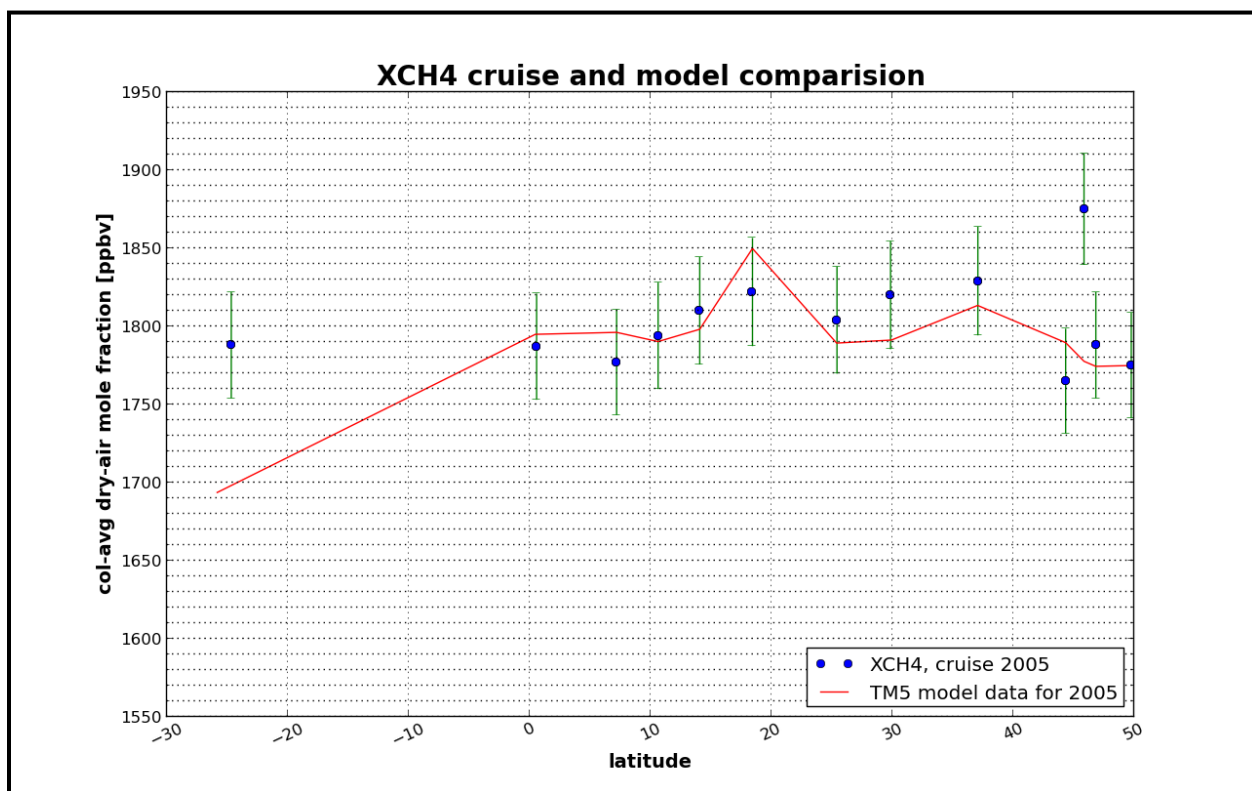


Figure 6.23: Retrieved methane from the ship cruise compared with TM5 model

Figure 6.24 depicts the comparison between the retrieved methane concentrations and the TM5 model. The error bars represent the diurnal variation of less than 2%. 90 % of the measurements showed diurnal variation less than 2 %. The diurnal variation means the absolute value of the deviation of one measurement from the daily mean. So, the diurnal variation was calculated as:

$$\text{diurnal variation} = \left(\frac{x}{\langle x \rangle} - 1 \right) \times 100 \quad (6.1)$$

Where,

x= one measurement

<x> = the mean of one day

On the other hand, the TM5 model data are given for particular latitude. As the comparison shows, our retrieved concentration agrees quite well with the model. The offset between the model and our measurements might be due the local source influence on our measurements. Besides, the model is modeled on a coarse resolution taking into account only the primary transport features. [Krol *et.al.*]. Retrieved methane concentration especially in the southern hemisphere show high concentration compared to the model. Comparing to cruise analysis of 2003 [Figure 6.23] , the concentration of methane in the southern hemisphere is higher in the analysis of cruise 2005. This supports the study of Petersen *et.al.*,(2010) which measured higher concentration of methane in the tropics in 2005.

6.6 Conclusion

Among the two spectroscopic line lists used during the study, the new line list gives a better quality of retrieval. It showed lower chi-square values compared to new line list which indicates a better fit between our calculated and measured spectrum. Using two different water vapour apriori did not have much impact on the retrieval based on the new line list. Two different water vapour apriori caused almost 10 % differences in the retrievals based on the old line lists. The impact of two water vapour apriori on the retrieval based on new line list was around 0.7 %. i.e. retrieval based on new line lists were almost independent of the water vapour apriori used. This also ensures the better quality of the retrieval based on new line lists compared to the old line list.

The analysis of cruise measurements of 2005 revealed higher concentration of methane in the tropics compared to the cruise measurements taken in 2003. The enhanced methane concentration in 2005 was also found by Petersen *et.al.* , (2010) during a measurement campaign. The average concentration of methane from the cruise 2005 analysis is 1802 ± 6 ppbv. Whereas, according to Petersen

et.al. (2010) the concentration of methane in the tropics during the measurement campaign in 2005 was 1790 ± 10 ppbv . The high concentration of methane was due to the higher influence of biomass burning sources. The study results from the cruise 2005 analysis agree quite well with the model data from TM5 inverse model. The reason for discrepancy between the model and the study results is assumed to be the influence of local biomass sources in the measurements and the simplified transport consideration by the model.

REFERENCES

BANWELL, C.N., 1996. *Fundamentals of molecular spectroscopy*. First edn. Great Britain: McGraw-Hill Publishing Company Limited

BERGAMASCHI, P., FRANKENBERG, C., MEIRINK, J.F., KROL, M., VILLANI, M.G., HOUWELING, S., DENTENER, F., DLUGOKENCKY, E.J., MILLER, J.B., GATTI, L.V., ENGEL, A. and LEVIN, I., 2009. Inverse modeling of global and regional CH₄ emissions using SCIAMACHY satellite retrievals. *Journal of Geophysical Research-Atmospheres*, **114**, pp. D22301.

CHANG, R., 1971. *Basic Principles of Spectroscopy*. First edn. United States of America: McGraw-Hill Book Company.

DEUTSCHER, N.M., GRIFFITH, D.W.T., BRYANT, G.W., WENNBERG, P.O., TOON, G.C., WASHENFELDER, R.A., KEPPEL-ALEKS, G., WUNCH, D., YAVIN, Y., ALLEN, N.T., BLAVIER, J.-., JIM'NEZ, R., DAUBE, B.C., BRIGHT, A.V., MATROSS, D.M., WOFYSY, S.C. and AND PARK, S., 2010. Atmospheric Measurement Techniques, **3**(947-958),.

DILS, B., DE MAZIERE, M., MÜLLER, J.F., BLUMENSTOCK, T., BUCHWITZ, M., DE BEEK, R., DEMOULIN, P., DUCHATELET, P., FAST, H., FRANKENBERG, C., GLOUDEMANS, A., GRIFFITH, D., JONES, N., KERZENMACHER, T., KRAMER, I., MAHIEU, E., MELLQVIST, J., MITTERMEIER, R.L., NOTHOLT, J., RINSLAND, C.P., SCHRIJVER, H., SMALE, D., STRANDBERG, A., STRAUME, A.G., STREMME, W., STRONG, K., SUSSMANN, R., TAYLOR, J., VAN DEN BROEK, M., VELAZCO, V., WAGNER, T., WARNEKE, T., WIACEK, A. and AND WOOD, S., 2006. Comparisons between SCIAMACHY and ground-based FTIR data for total columns of CO, CH₄, CO₂ and N₂O. *Atmospheric Chemistry and Physics*, **6**(1953–1976),.

DLUGOKENCKY, E.J., STEELE, L.P., LANG, P.M. and MASARIE, K.A., 1994. The growth rate and distribution of atmospheric methane. *Journal of Geophysical Research*, **99**(94JD01245),.

FORSTER, P., RAMASWAMY, V., ARTAXO, P., BERNTSEN, T., BETTS, R., FAHEY, D., HAYWOOD, J., LEAN, J., LOWE, D., MYHRE, G., NGANGA, J., R. PRINN, G. RAGA, M. S., AND DORLAND, R. V.: 1..FORSTER, P., RAMASWAMY, V., ARTAXO, P., BERNTSEN, T., BETTS, R., FAHEY, D., HAYWOOD, J., LEAN, J., LOWE, D., MYHRE, G., NGANGA, J., R. PRINN, G. RAGA, M. S., AND DORLAND, R. V.:, *Changes in Atmospheric Constituents and in Radiative Forcing, Climate Change 2007: The Physical Science Basis. Contribution of Working Group I to the Fourth Assessment Report of the Intergovernmental Panel on Climate Change (IPCC)*, 2007. .

FRANKENBERG, C., BERGAMASCHI, P., BUTZ, A., HOUWELING, S., MEIRINK, J.F., NOTHOLT, J., PETERSEN, A.K., SCHRIJVER, H., WARNEKE, T. and AND ABEN, I., 2008. Tropical methane emission: A revised view from SCIAMACHY onboard ENVISAT. *GEOPHYSICAL RESEARCH LETTERS*, **35**(L15811),.

KROL, M., HOUWELING, S., BREGMAN, B., VAN DEN BROEK, M., SEGERS, A., VAN VELTHOVEN, P., PETERS, W., DENTENER, F. and BERGAMASCHI, P., 2005. *The two-way nested global chemistry zoom model TM5: algorithm and applications. Atmospheric Chemistry and Physics*, **4**(417-432),.

MENKE, W., 1989. *Geophysical Data analysis: Discrete Inverse Theory. Revised edition edn. The United States of America: Academic Press.*

NOTHOLT, J., TOON, G.C., RINSLAND, C.P., POUGATCHEV, N.S., JONE, N.B., CONNOR, B.J., WELLER, R., GAUTRIOIS, M. and SCHREMS, O., 2000. *Latitudinal variation of trace gas concentration in the free troposphere measured by solar absorption spectroscopy during a ship cruise. Journal of Geophysical Research*, **105**(1337-1349),.

PALM, M., 2013, *Personal Communication* (mathias@iup.physik.uni-bremen.de).

PETERSEN, A.K., WARNEKE, T., FRANKENBERG, C., BERGAMASCHI, P., GERIB, C., NOTHOLT, J., BUCHWITZ, M., SCHNEISING, O. and AND SCHREMS, O., 2010. *First ground-based FTIR observations of methane in the inner tropics over several years. Atmospheric Chemistry and Physics*, **10**(7231–7239),.

RODGERS, C.D., 2000. *INVERSE METHODS FOR ATMOSPHERIC SOUNDING Theory and Practice. Singapore: World Scientific Publishing Co.Pte.Ltd.*

ROTHMAN, L.S., GORGON, I.E., BARBE, A., CHRIS BENNER, D., BERNATH, P.F., BIRK, M., BOUDON, V., BROWN, L.R., CAMPARGUE, A., CHAMPION, J.P., CHANCE, K., COUDER, L.H., DANA, V., DEVI, V.M., FALLY, S., FLAUD, J.M., GAMACHE, R.R., GOLDMAN, A., JACQUEMART, D., KLEINER, I., LACOME, N., LAFFERTY, W.J., MANDIN, J.Y., MASSIE, S.T., MIKHAILENKO, S.N., MILLER, C.E., MOAZZEN-AHMADI, N., NAUMENKO, O.V., NIKITIN, A.V., ORPHAL, J., PEREVALOV, V.I., PERRIN, A., PREDOI-CROSS, A., RINSLAND, C.P., ROTGER, M., SIMECKOVA, M., SMITH, M.A.H., SUNG, K., TASHKUN, S.A., TENNYSON, J., TOTH, R.A., VANDAELE, A.C. and AND VANDER-AUWERA, J., 2009. *The HITRAN 2008 molecular spectroscopic database. Journal of Quant. Spectrosc. Ra*, **110**(533-572),.

SCHNEISING, O., BUCHWITZ, M., BOVENSMANN, H., BERGAMASCHI, P. and AND PETERS, W., 2009. *Three years of greenhouse gas column-averaged dry air mole fractions retrieved from satellite-Part 2: Methane. Atmospheric Chemistry and Physics*, **9**(443-465),.

SEPULVEDA, E., SCHNEIDER, M., HASE, F., GARCIA, O.E., GOMEZ-PELAEZ, A., DOHE, S., BLUMENSTOCK, T. and AND GUERRA, J.C., 2012. *Long-term validation of tropospheric column-averaged CH₄ mole fractions obtained by mid-infrared ground-based FTIR spectrometry. Atmospheric Measurement Techniques*, **5**(1425-1441),.

SUSSMANN, R., FORSTER, F., RETTINGER, M. and JONES, N., 2011. *Strategy for high-accuracy-and-precision retrieval of atmospheric methane from the mid-infrared FTIR network. Atmospheric Measurement Techniques Discussions*, **4**(2695-3015),.

VELAZCO, V., NOTHOLT, J., WARNEKE, T., LAWRENCE, M., BREMER, H., DRUMMOND, J., SCHULZ, A., KRIEG, J. and SCHREMS, O., 2005. Latitude and altitude variability of carbon monoxide in the Atlantic detected from a ship-borne Fourier transform spectrometry, model, and satellite data. *Journal of Geophysical Research*, **110**(D09306),.

WARNEKE, T., MEIRINK, J.F., BERGAMASCHI, P., GROOß, J.U., NOTHOLT, J., TOON, G.C., VELAZCO, V., GOEDE, A.P.H. and AND SCHREMS, O., 2006. Seasonal and latitudinal variation of atmospheric methane: A ground-based and ship-borne solar IR spectroscopic study. *GEOPHYSICAL RESEARCH LETTERS*, **33**(L14812),.